AIMS Materials Science, 12(3): 514–561.
DOI: 10.3934/matersci.2025024
Received: 13 April 2025
Revised: 21 May 2025
Accepted: 04 June 2025
Published: 27 June 2025

http://www.aimspress.com/journal/Materials

Research article

Synergistic effect of chemically modified CNC nanofiller concentration on the mechanical and thermal properties of additively manufactured PLA-TPU-CNC composites

Paul Eric C. Maglalang[1,2] and Blessie A. Basilia[1,*]

[1] School of Chemical, Biological, and Materials Engineering and Sciences, Mapúa University, 658 Muralla St., Intramuros Manila, 1002 Philippines
[2] Industrial Technology Development Institute—Department of Science and Technology (DOST), Compound General Santos Avenue, Bicutan, Taguig City, 1631 Philippines

* **Correspondence:** Email: babasilia@mapua.edu.ph; Tel: +63-917-591-3372.

Abstract: The continual application of renewable cellulose nanoparticles has led to several advancements in their performance as a reinforcing component for the fabrication of high-performance additively manufactured nanocomposite products. Nonetheless, incorporating hydrophilic cellulose nanocrystals into hydrophobic thermoplastics, such as polylactic acid and thermoplastic urethane, remains a substantial challenge for achieving successful and smooth compatibility as an additional component in 3D-printed composites. This study has successfully investigated the effects of chemically modified cellulose nanocrystals at concentrations of 0.05%, 1%, and 3% when blended with hexadecyltrimethylammonium bromide and polylactic acid-thermoplastic urethane (PLA-TPU) at an 80:20 ratio. This study demonstrates the use of a fused deposition modeling (FDM) printer to manufacture 3D-printed PLA-TPU-CNC (cellulose nanocrystal) composites through additive manufacturing. The composite with 0.05% modified CNC exhibits 19.12 MPa higher tensile strength and 58.3% higher flexural strength than the unmodified one. Furthermore, the PLA-TPU blend with 1% modified CNC obtained the highest Izod impact strength, 63.43 MPa. The 3D-printed composite with 1% modified CNC displayed significantly better compressive strength than other modified variations and concentrations in the unmodified group. Composites with 1% unmodified CNC exhibited 2.33% higher heat deflection than blended PLA-TPU. The composites with 0.05% modified CNC showed an increase of 1.12% compared to the PLA-TPU blend and a modest increase of up to 2.71% compared to the other modified CNC concentrations. The composite with 1% modified

CNC was superior to all the variations in terms of hardness, with a 29.6% increase above the 1% unmodified composite. The utilization of cationic surfactants, such as hexadecyltrimethylammonium bromide (HDTMA-Br), enhances CNC infiltration, interfacial adhesion, and hydrophobicity control, thereby improving the mechanical performance of the composites and making them suitable for specific medical and engineering material designs and applications. The F-statistics for all concentration levels yielded a ratio substantially greater than the F-critical value, and the p-value was considerably less than 0.05, indicating a significant and favorable design criterion.

Keywords: polylactic acid (PLA); thermoplastic urethane (TPU); cellulose nanocrystal (CNC); hexadecyltrimethylammonium bromide (HDTMA-Br); surface modification; interfacial adhesion; 3D printing/additive manufacturing (AM); fused deposition modeling (FDM)

1. Introduction

Additive manufacturing (AM) has transformed industrial, engineering, construction, aerospace, education, and medical sectors [1–3]. Fused deposition modeling (FDM) is a simple, cost-effective, extrusion-based 3D printing process. To make a three-dimensional structure, a heated nozzle melts, extrudes, and layers material filaments onto a build plate. Manufacturing materials without moulds or templates is easy. Many businesses use FDM for 3D printing nanocomposite materials due to its design and manufacturing flexibility. Adjusting temperature, printing speed, layer thickness and width, printing direction, raster angle, and layer overlap can enhance the properties of 3D-printed materials. These properties enable seamless printing of precise multilayer structures [1–3]. Although limited, FDM-based 3D printing is available. Under-extrusion, over-extrusion, and warping impact the mechanical properties of FDM polymers, limiting their use in 3D printing [4]. Most typically used with thermoplastics such as polylactic acid (PLA) and thermoplastic urethane (TPU), FDM is a low-cost and suitable option for quick prototyping [1,3]. Polylactic acid and thermoplastic urethane work better in FDM printers than single filaments [3].

3D printing orthopedic devices with biodegradable polymers like PLA is biocompatible and biosafe. PLA's tensile strength and brittleness exceed those specified in ISO 10328 [5]. TPU increases PLA's tear resistance and flexibility. This interaction enhances the composite's mechanical and thermal properties [4,6,7]. Blended PLA-TPU meets design requirements with outstanding mechanical qualities [2]. Moreover, increased strain from TPU and PLA increases resistance. TPU strengthens and rigidifies the composite, enabling it to excel in toughness tests [2–4]. However, most PLA-TPU compounds have printing-induced micro-holes and cavities that are hard to remove. Rapid raster cooling shrinks nearby rasters and layers in printing parts, causing poor connections. These voids are the primary cause of FDM porosity [8–10]. Micro-voids weaken interfaces [11,12]. These voids cause most strength loss due to localized stresses and porosity [13]. Extruding more molten material reduced holes with higher feeding rates and FDM gear rotating speed [14].

Cellulose nanocrystal (CNC) matrix mixing improves polyurethane (PU) foam's reinforcing, surface bonding, and thermal properties. Filler reinforcement in 3D-printed PLA composites minimizes voids and boosts flexibility. Nanocellulose smooths PLA and TPU surfaces by sealing small extrusion holes, preventing voids, and reducing porosity. Graphene oxide improves the mechanical and thermal properties of nanocomposites. However, the connection between PLA, TPU, and cellulose

is weak due to opposing chemical properties. Incompatibility between PLA, TPU, and CNC composites affects dispersion and interfacial adhesion, thereby impacting the mechanical and thermal properties. Few CNC investigations have been conducted on PLA-TPU-CNC blend nanocomposites. Graphene oxide enhances the characteristics of polymer mixtures, and additive manufacturing (AM) approaches can facilitate the investigation of TPU/PLA/GO (graphene oxide) nanocomposite applications [1–3,7].

Cellulose nanocrystals can replace synthetic nanomaterials, such as carbon nanotubes, as matrix reinforcements, thereby improving the mechanical properties of composites. They work with changed nanoparticle surfaces, reducing moisture absorption [1] and making them a good synthetic nanomaterial. When added to polymers, cellulose nanocrystals strengthen surfaces, while surface-active chemicals stabilize them [15]. The combination of TPU and PLA enhances the strain, thereby strengthening the composites. Polylactic acid and thermoplastic urethane make it easy to add fillers and reinforce composites. A good PLA-TPU combination makes 3D-printed designs mechanically sound [16–18]. However, hydrophobic polymers may prevent evenly dispersed hydrophilic nanoparticles, making composites brittle. Some studies underestimate the impact of nanoparticles on PLA-TPU, and there is a lack of research on the integration and orientation of natural nanoparticles in 3D-printed transtibial prosthetic socket composites [5,19,20].

According to Ambone et al., 3D-printed PLA composites with filler are more flexible, have fewer cavities, and exhibit less agglomeration. A proper filler concentration prevents material agglomeration. Composite crystallinity, strain, and brittleness increase with the addition of nanofillers [1,21–24]. CNC mixing with the matrix results in a wider and more stable nanoparticle dispersion, which enhances matrix surface bonding throughout, thereby improving both mechanical and thermal properties [1,25–27]. Some surface-active chemicals can increase the zeta potential and matrix stability of cellulose nanoparticles [24]. Kaboorani et al. repeatedly replaced hydroxyl ions with small particles to convert hydrophilic cellulose nanocrystals into hydrophobic nanoparticles. Results showed hexadecyltrimethylammonium bromide (HDTMA-Br) stabilizes CNC. Concentration regulates CNC hydrophobicity [28,29]. Kaboorani et al. observed that HDTMA-Br may affordably change CNC surfaces, which is promising. In diverse settings, altering CNC with HDTMA-Br did not affect its X-ray patterns; therefore, its crystallite structure remained unchanged [15].

Here, we explore the impact of CNC concentrations on the mechanical and thermal properties of PLA-TPU composites. We exclusively examined HDTMA-Br as the sole surface-active agent, as introduced by Kaboorani et al. To enhance the interfacial cohesive adhesion of CNC, and given the absence of detrimental effects from this cationic surfactant, the study opted for HDTMA-Br/cetyltrimethylammonium bromide (CTAB), which increases the hydrophobicity and compatibility of CNC when combined with hydrophobic matrices. A filament production machine creates a smooth and adequately prepared filament for 3D printing according to specified requirements [30,31]. Utilizing a fused deposition modeling printer, we investigate the effects of chemically modified and unmodified CNC at concentrations of 0.05%, 1%, and 3% on the mechanical and thermal properties of additively built PLA-TPU blends.

2. Materials and methods

2.1. Summary of experimental workflow

The study's experimental workflow, illustrated in Figure 1, involves material selection, preparation of composite materials, 3D printing, characterization of CNCs and 3D-printed specimens, mechanical testing, and data analysis. Each stage is essential for ensuring the dependability and correctness of the outcomes.

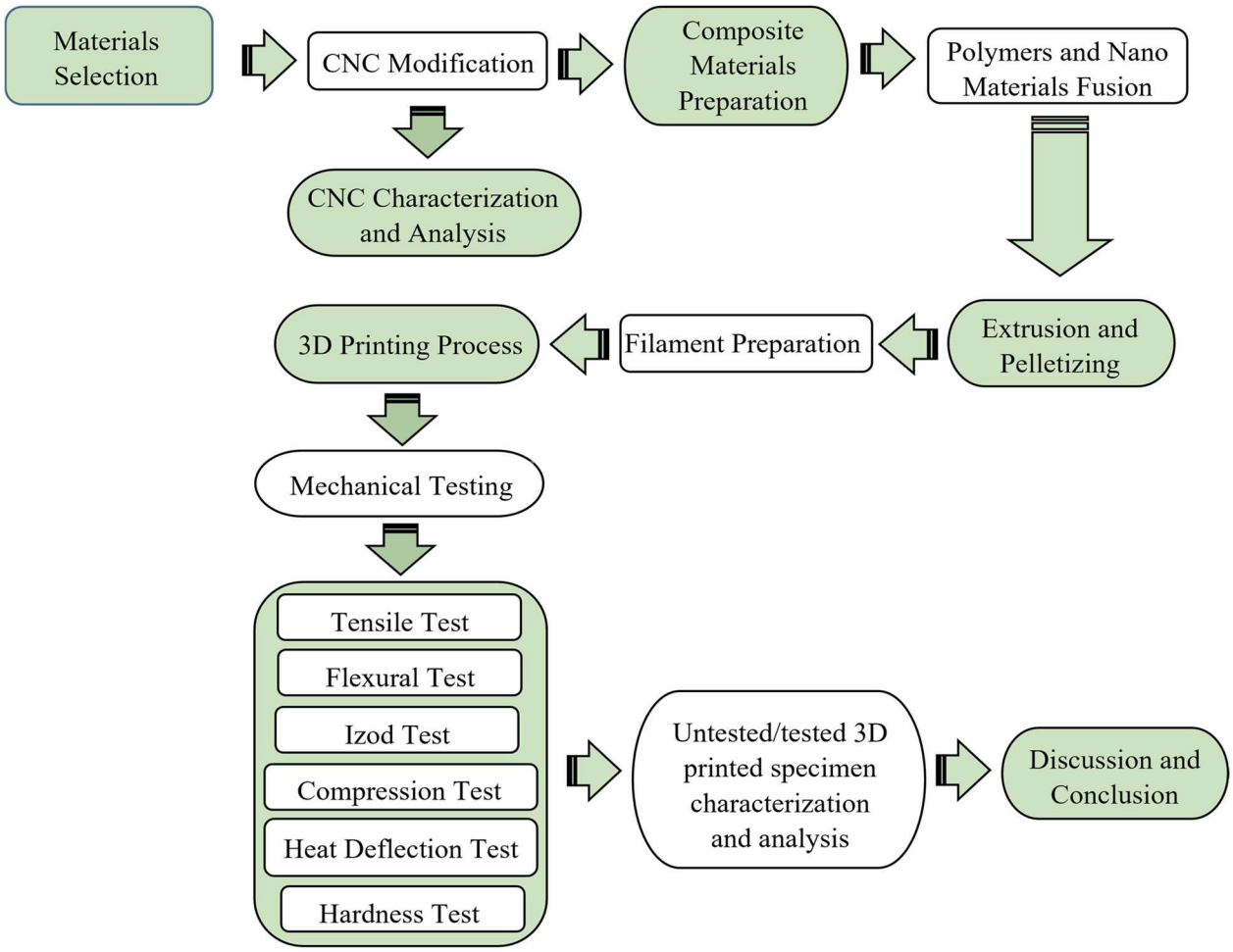

Figure 1. Experimental workflow.

Material selection: we incorporate PLA, TPU, and commercial CNC powder. The PLA-TPU ratio was based on our design of experiments (DOE) of 80:20. Furthermore, a cationic surfactant, CTAB, also known as HDTMA-Br, was employed to enhance the CNC's compatibility with polymers.

CNC modification with HDTMA-Br: a 20 g batch of spray-dried CNC and a 10 g batch of HDTMA-Br powder, blended with water at 25 °C for at least 4 h, were rinsed with deionized water. The mixture was then deposited into a vial and centrifuged to prepare it for freeze-drying, yielding a modified nano-powder CNC.

Composite materials preparation: to ensure adequate CNC dispersion, a master batch of the sample is manufactured at an 8% weight percentage. Before extrusion and pelletizing using a

co-rotating twin-screw extruder at temperatures ranging from 150 to 170 °C, the CNC concentration is blended with pure PLA-TPU powder in a 20:80 ratio.

3D printing process: the experiment's design required the fabrication of filaments for the unmodified and modified CNC with fiber concentrations of 0.05%, 1%, and 3%. The nozzle diameter is 0.60 mm, which is ideal for preventing blockage and the uncontrolled release of extruded filament material during 3D printing. Examining related literature led to the selection of default values for raster angle, overlapped width, and layer height. They are useful for smooth printing, particularly with PLA materials. The extrusion speed, nozzle, and build plate temperature values were chosen since they are currently standard for printed PLA materials [30,31]. The 20% infill density and honeycomb design were picked to save printing time while producing high-quality printing material.

Characterization of materials: the unmodified and modified CNCs were characterized using Fourier Transform Infrared Spectroscopy (FTIR), Thermogravimetry Differential Thermal Analysis (TG-DTA), Differential Scanning Calorimetry (DSC), X-ray Diffraction (XRD), and Transmission Electron Microscopy (TEM). The morphological structure of the 3D-printed specimens was also determined using Scanning Electron Microscopy (SEM) and Energy-Dispersive X-ray Spectroscopy (EDX) imaging, as well as Atomic Force Microscopy *(*AFM) imaging.

Mechanical testing: mechanical tests, including tensile, flexural, impact, compression, heat deflection, and hardness tests, are employed to evaluate the performance of the prepared specimens.

Data analysis and processing: the mechanical testing results of unmodified and modified composite specimens are evaluated and compared to those of a typical PLA-TPU sample. This analysis facilitates understanding the improvements in mechanical characteristics and the potential mechanisms underlying them.

The following subsections provide a comprehensive description of the study's methodology, delving deeper into the workflow outlined in Figure 2.

2.1. Material selection, CNC modification, composite, and filament preparation

In this study, 98 wt% spray-dried CNCs, 5–20 nm wide and up to 250 nm long, at a density of 1.50 g/cm^3, with an aspect ratio of 31 and a crystallinity index of 89%, were purchased from Cellulose Lab Inc., Fredericton, Canada. Additionally, HDTMA-Br/CTAB (57-09-0), with a purity of ≥99%, a pH range of 5–9, and soluble in both water and alcohol, has a melting point (Tm) of 243 °C. It was purchased from Wuxi Philchem New Materials Co., Ltd. In addition, pure polylactic acid pellets (PLA BC2003RE) locally supplied by First in Colours Inc., Philippines, have a density ranging from 1.25 to 1.36 g/cm^3, a glass transition temperature (Tg) ranging from 55 to 60 °C, and a melting point of 150 to 180 °C. Moreover, the thermoplastic polyurethane (TPU 90A SP502 powder, 120 μm) having a hardness ranging from 88 ± 2 Shore A, a melting point of 120–156 °C, a glass transition of −20 ± 10 °C, and a density of 1.21 g/cm^3 was provided by Guangdong Silver Age Science and Technology Co., Ltd.

As shown in Figure 2, the extraction of modified CNC was performed using a centrifuge, with each 15-min centrifugation step conducted at 25 °C and 7000 rpm. Thorough washing with deionized water was performed to eliminate any probable excess of ammonium salts caused by CNC surface aggregation. Ten sets of a solution mixture were centrifuged per batch and then stored in a freezer, model ESCO/UUS-363A-3-5D-SS, for at least 48 h at −70 °C before being placed in a freeze-dryer

oven model Gamma 2-16 LSC plus, with a freeze-drying temperature of –35 °C at 0.20 millibar pressure for at least 2 days to dry the mixture thoroughly.

Before the 3D-printing process, a corotating twin-screw extruder at 150–170 °C and 8 rpm extruded 500 g of an 80:20 pelletized mixture of PLA and TPU. Moreover, 500 g master batch samples containing 8% CNC blended with PLA and TPU pellets/powder (80:20) were also employed and extruded using a machine. The compounded master batch was mixed with pelletized PLA + TPU (80:20) to produce a blended PLA-TPU-CNC at 0.05%, 1%, and 3% concentrations and fed into a single extrusion machine (3D Devo filament maker) operating at 170–180 °C, 5.50 rpm to form a 1.75 mm diameter filament.

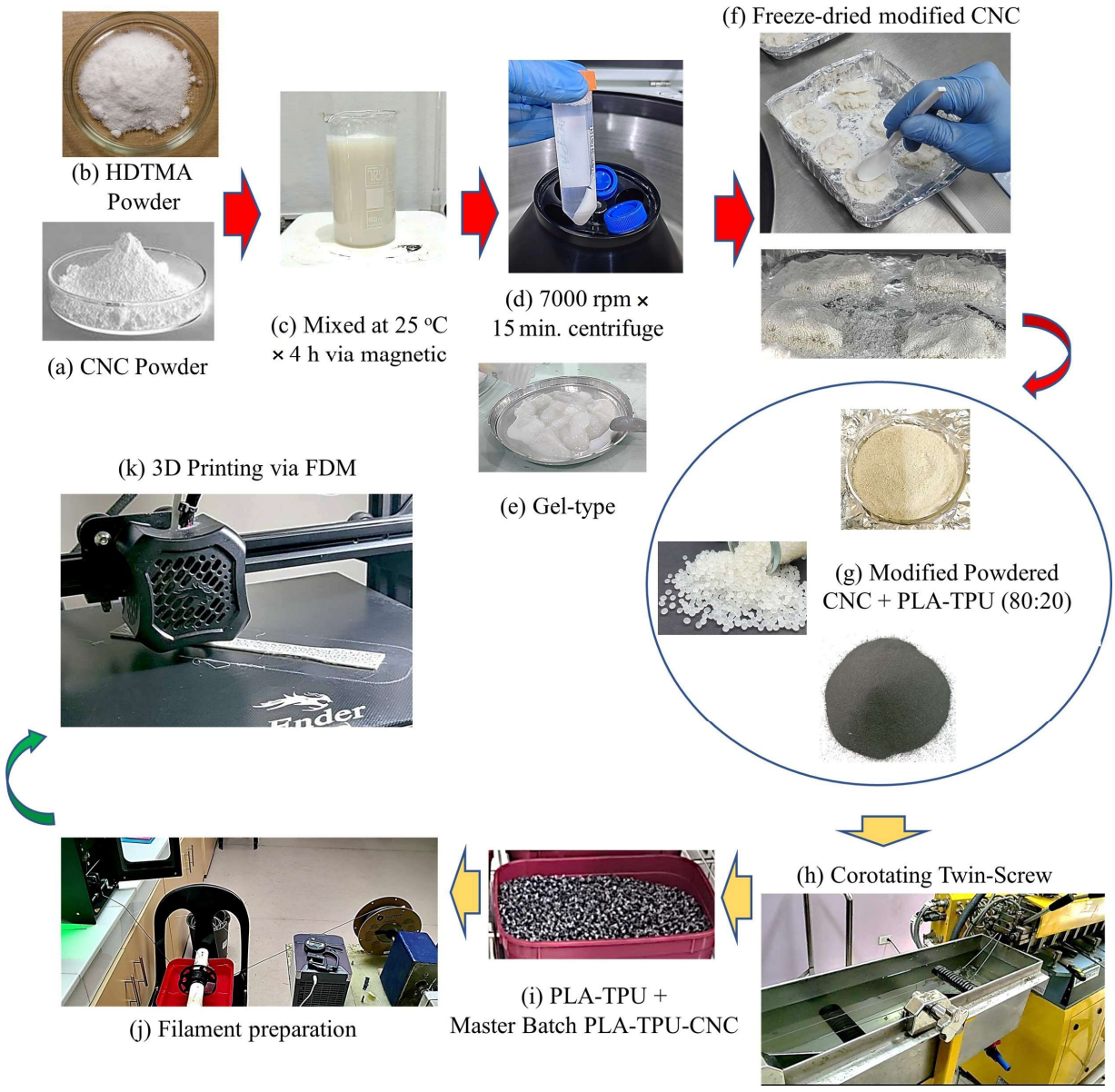

Figure 2. CNC surface modification: (a) pristine CNC powder; (b) HDTMA powder; (c) CNC-HDTMA mixed; (d) CNC-HDTMA centrifuge; (e) gel-type CNC-HDTMA; (f) freeze-drying; (g) PLA-TPU blend with surface-modified CNC; (h) twin-screw extrusion; (i) pelletized PLA-TPU-CNC; (j) filament preparation; (k) 3D-printing.

2.2. Additive manufacturing via FDM

All the specimens were 3D printed on an FDM machine in a flatwise orientation with the default printing parameters listed in Table 1.

Table 1. FDM 3D-printing parameters.

Parameters	Value
A. Diameter of nozzle, mm	0.60
B. Raster angle, º	45
C. Perimeters overlapped, %	55
D. Raster width, mm	0.40
E. Layer height, mm	0.20
F. Extrusion speed, mm/s	50–60
G. Nozzle temperature, ℃	230
H. Build plate temperature, ℃	60
I. Infill density, %	20
J. Infill pattern	Honey-comb

2.3. Material characterization and physical testing

The Infrared (IR) spectra and thermographs of the unmodified and modified CNC were analyzed using a PerkinElmer FTIR Frontier spectrometer and a Thermal Analyzer, respectively. The crystallite structure was also investigated using an X-ray diffractometer. TEM images were examined using the JEOL JEM 2100F and ImageJ software. The SEM-EDX image and spectra of the CNC-structured composite, incorporating CNC, were studied using the FEI HELIOS NANOLAB 600i. The AFM surface roughness of the unmodified and modified 3D-printed specimens was captured using the Park System's AFM Model XE-100. The mechanical properties were tested using an Instron 5585H, Shimadzu AGS-50kNXD, Zwick/Roell 5.5P, Amsler HDT/Vicat, and Hildebrand Digital Durometer Model HDD-2.

2.4. FTIR analysis

An analytical method for identifying organic, polymeric, and, in some situations, inorganic compounds. FTIR analysis scans test samples and observes chemical characteristics using infrared light. The Perkin Elmer FTIR Frontier characterized the IR spectra of unmodified and modified CNC. Fourier Transform Infrared Spectroscopy was used to examine the original and modified CNC samples after they were oven-dried at 50 °C for 24 h to remove any moisture content. Using the transmittance mode, the FTIR spectra of the materials were analyzed in the 4000–500 cm^{-1} region.

2.5. TG-DTA analysis

A thermal analyzer that can measure and characterize multiple thermal parameters of a sample simultaneously, the TG part tracks the temperatures at which oxidation, reduction, or breakdown occur.

The CNC-powdered sample used in the study was evaluated using a thermal analyzer (TG-DTA) from PerkinElmer STA 6000. This device has a balancing resolution of 0.1 μg, which is temperature-dependent. Heating rates ranged from 30 to 900 °C at a rate of 10.00 °C/min, with a holding time of 4.0 min at 900 °C under high-purity nitrogen at a flow rate of 20 mL/min.

2.6. DSC analysis

Thermal analysis measures heat flow in a sample as its temperature changes. It enables researchers to study thermal transitions, such as melting, crystallization, or the glass transition, and determine key properties, including the melting point, heat of fusion, and glass transition temperature. The thermal transition and behavior of the composite were investigated using a Hitachi STA200RV Differential Scanning Calorimeter to determine the effect, impact, and thermal stability of unmodified and modified CNCs integrated into the PLA-TPU blend.

2.7. XRD analysis

This non-destructive analytical approach examines the physical properties of powder, solid, and liquid materials, including phase composition, crystal structure, and orientation. The crystallite structure was investigated using X-ray diffraction with Shimadzu XRD 6000 equipment to further explore the effects of CNC as an enhancement to the PLA-TPU matrix. The scanning rate was 1 °C/min, and the Cu-Kα radiation source (λ = 1.54060 Å) was operated at 40 kV and 30 mA. The XRD patterns were acquired within an angular range of 2 to 70°.

2.8. TEM analysis

This technique utilizes an electron beam to generate high-resolution images of objects, including their internal features at the nanoscale. The samples were sonicated in ultra-pure water for 10 min, then placed on Ted Pella Ultrathin C Film on Holey Carbon Support Film. The JEOL JEM-2100F Field Emission Transmission Electron Microscope, equipped with an Oxford Instruments X-Max 80T EDS detector, was used to obtain test findings specific to the lab sample. The current study utilized ImageJ software to analyze CNC TEM images to measure cellulose diameter and length.

2.9. SEM-EDX analysis

A SEM may generate various signals by sending a stream of high-energy electrons onto the surface of solid specimens. Electron-sample interactions reveal information on the sample's chemical composition, crystalline structure, orientation, and external morphology (texture). The SEM-EDX image and spectra of the CNC structure embedded in the 3D-printed composite were analyzed using the FEI HELIOS NANOLAB 600i.

2.10. AFM analysis

Advanced scanning probe microscopy enables atomic- or nanometer-scale surface imaging. Its operating idea is to measure the force interactions between a small probe tip and the sample surface.

3D-printed specimens were analyzed using Park System's Atomic Force Microscope Model XE-100.2. A scan size of 25 × 25 μm was used in non-contact mode, where the measured values of roughness are valid for the given scan size due to the sample's non-uniformity.

2.11. Tensile test

Tensile testing was performed on the 3D-printed composite samples under the ASTM D638 Type IV standard. The tests were conducted using the Shimadzu AGS-50kNXD universal testing machine (UTM), which is outfitted with a 1 kN load cell.

Specimens with the dimensions depicted in Figure 3 were subjected to a longitudinal tensile loading at a continuous crosshead speed of 5 mm/min until they ruptured. The maximum tensile strength and strain at break were all measured.

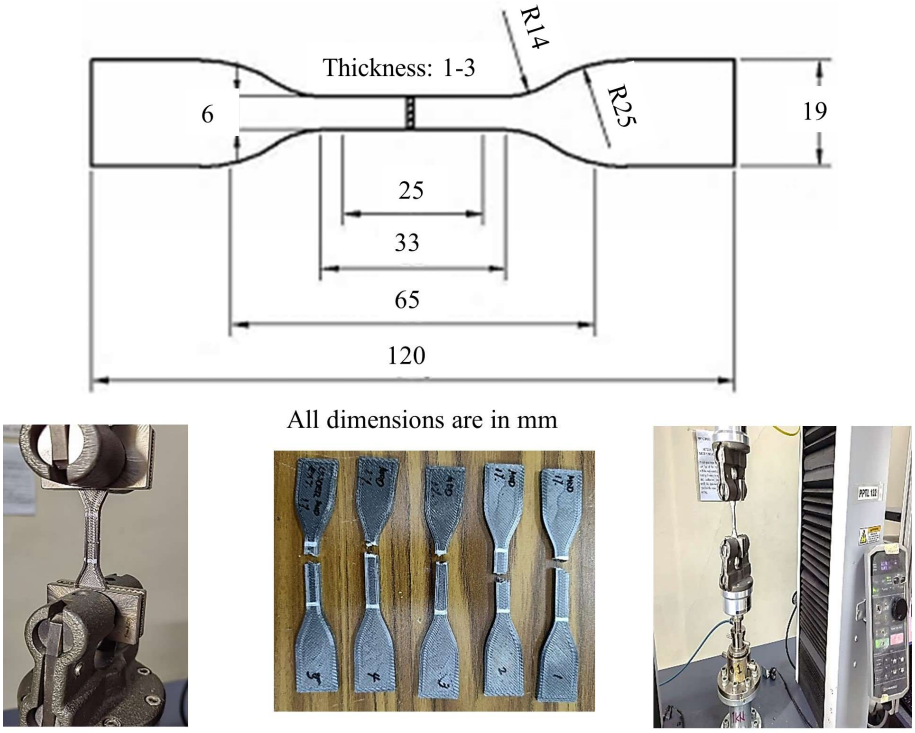

Figure 3. Tensile test.

2.12. Flexural test

The material's flexural behavior was measured using a three-point bending fixture. Figure 4 illustrates the dimensions of specimens designed according to the ASTM D790 standard. The test was performed using a Shimadzu AGS-50kNXD universal testing machine fitted with a 1 kN load cell.

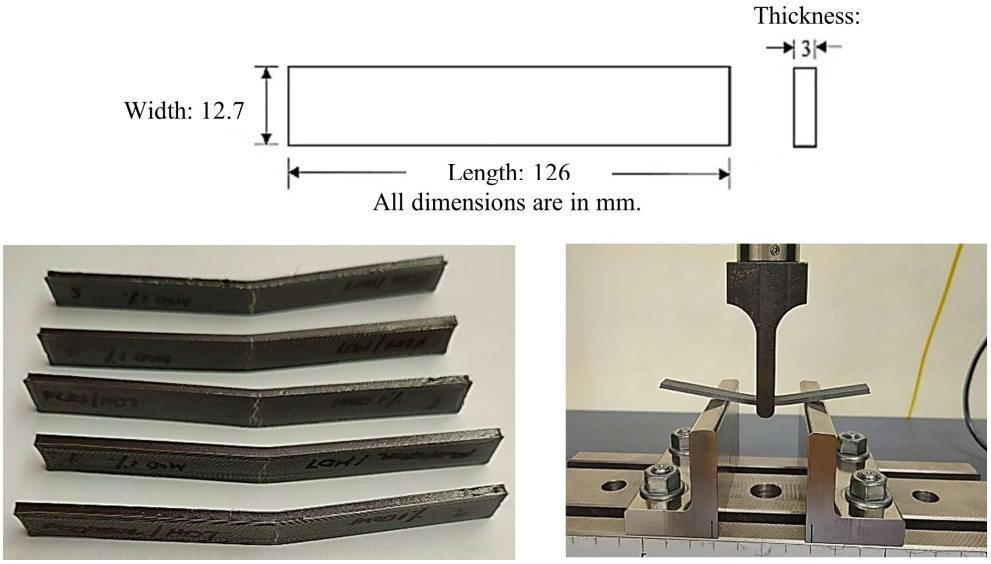

Figure 4. Flexural test.

2.13. Izod impact test

The specimens' impact energy was measured using Zwick/Roell 5.5P impact testing equipment to assess the material's ability to absorb rapid pressures and resist fracture, as illustrated in Figure 5.

Impact testing provides valuable information about the material's toughness and its ability to withstand dynamic loading conditions. The ASTM D256 standard was used to create the impact test specimens, which have the dimensions shown in Figure 5. The specimens were prepared by integrating CNC concentrations of 0.05%, 1%, and 3%.

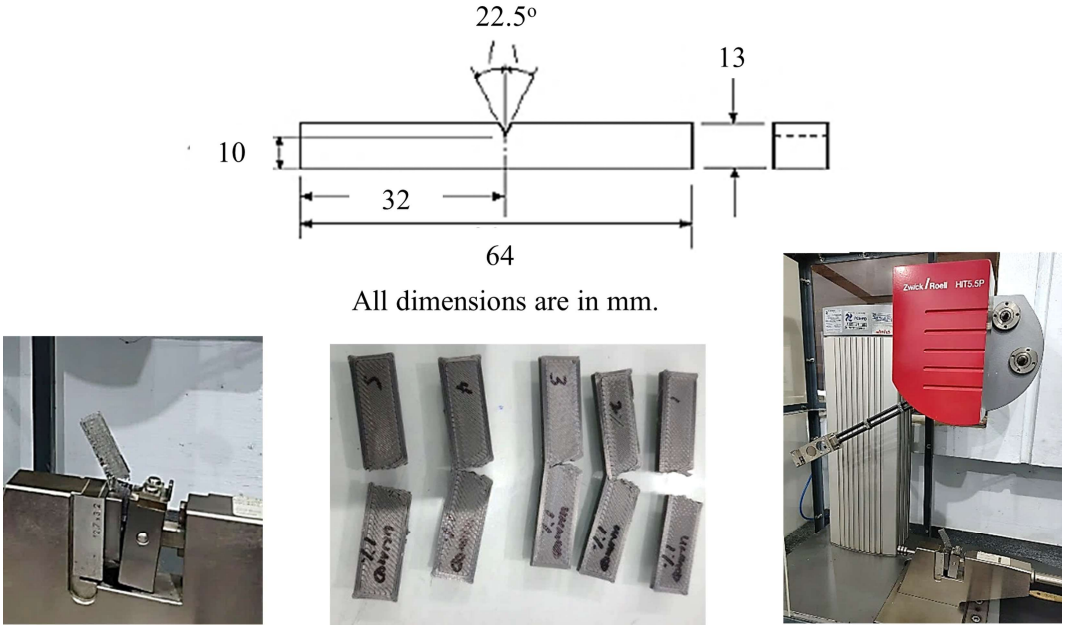

Figure 5. Izod impact test.

2.14. Compression test

A compressive force is applied to a test specimen according to ASTM D695, using a prismatic, rectangular, or cylindrical form, with a compression plate mounted on a universal testing machine to measure the material's behavior under applied crushing pressures. In Figure 6, the test was then performed using a Shimadzu AGS-50kNXD universal testing machine fitted with a 1 kN load cell.

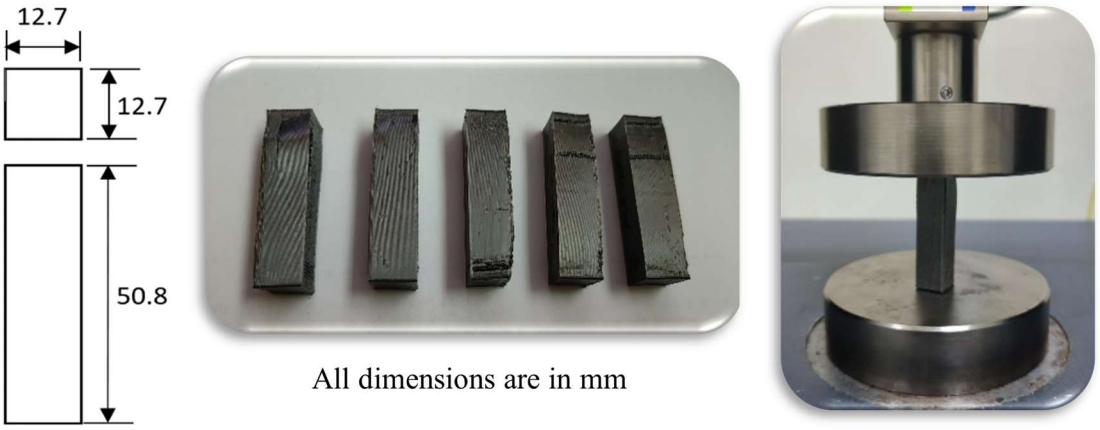

Figure 6. Compression test.

2.15. Heat deflection test

An evaluation of the degree to which a polymer or plastic material undergoes deformation under an applied force at a specific temperature, as per ASTM D648. The heat deflection test, as presented in Figure 7 for the given samples in this study, was evaluated using a Zwick Roell Amsler HDT instrument with a display accuracy of 300 °C and a 0.01 °C resolution.

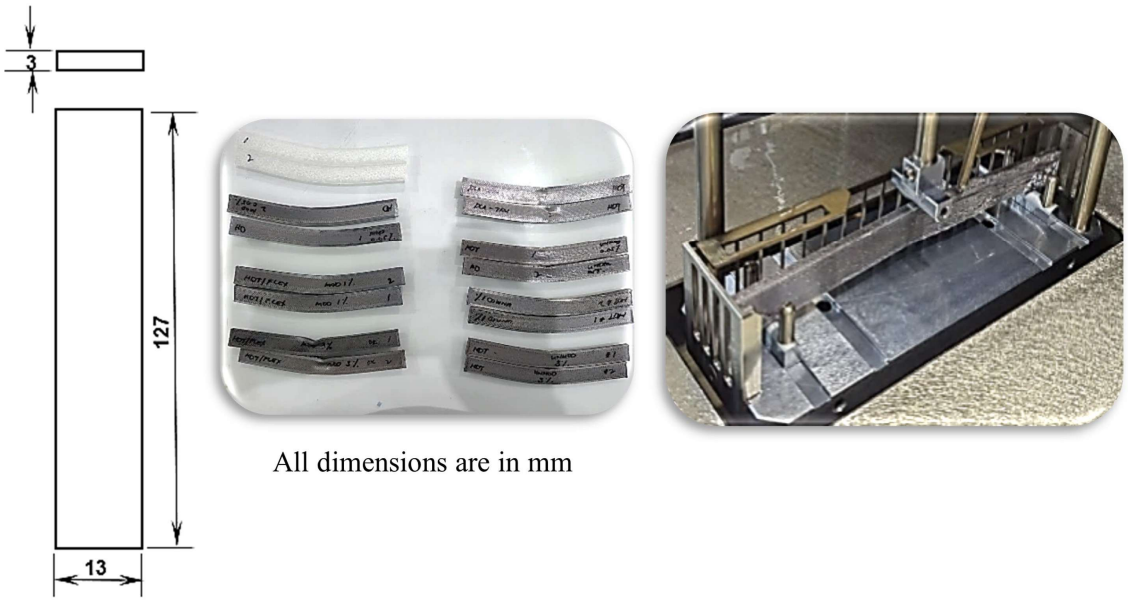

Figure 7. Heat deflection test.

2.16. Hardness test

Hardness is a mechanical test that determines the extent to which a material can be penetrated without being damaged. It can also evaluate a material's strength, wear resistance, and other mechanical qualities. In Figure 8, the test was performed using a Hildebrand Digital Durometer Model HDD-2, which has ±0.5 accuracy and 0.1 resolution and conforms to ISO 868 and ASTM D2240 standards.

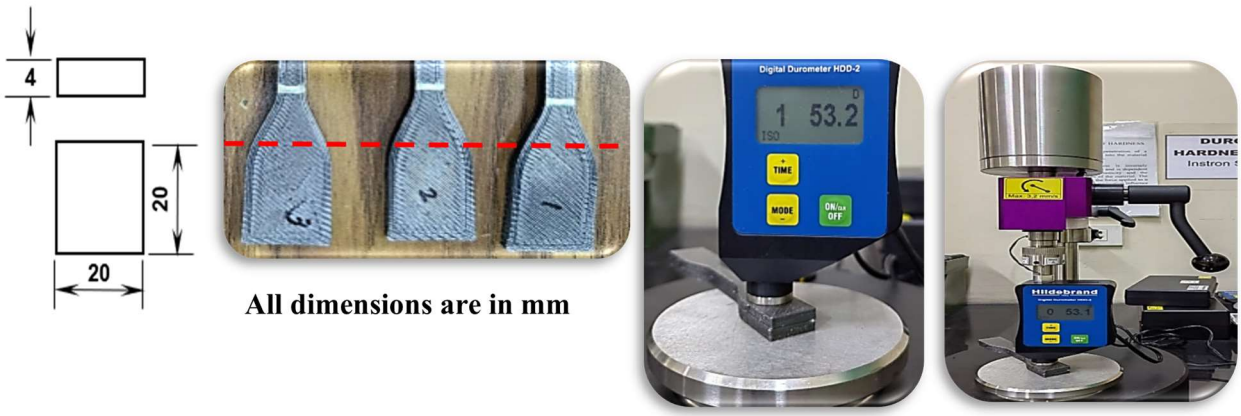

Figure 8. Hardness test.

3. Results and discussion

3.1. FTIR analysis

The FTIR spectra of the unmodified and modified CNCs were characterized, as shown in Figure 9a,b. In addition, an intensity of 1640.31 and 1639.85 cm^{-1} was detected for unmodified and modified CNC, respectively, indicating the presence of double bonds or aromatic compounds. Peaks between 1200 and 1400 cm^{-1} were also observed for both modified and unmodified CNC, confirming the presence of an OH bending mode [32–35]. Furthermore, most of the peaks associated with the ether group of the unmodified and modified CNC were identified in the 800–1150 cm^{-1} range, indicating the presence of alkyl and aromatic C–O stretches [36].

3.1.1. FTIR spectra analysis for unmodified CNC

A broad absorption band of unmodified CNC, occurring from 3250 to 3650 cm^{-1}, was observed in the OH stretch area, indicating the presence of hydrogen bonding and, thus, the presence of water [24]. The functional group associated with the alkane C–H stretch was visible at a peak of 2893.58 cm^{-1}, and the absorption band at 2935–2860 cm^{-1} revealed a long-chain, linear aliphatic molecule.

3.1.2. FTIR spectra analysis for modified CNC

However, the absorption band of the modified CNC in the same range was relatively higher than that of the unmodified CNC, yielding an absorption band of 3335.71 cm^{-1} in the OH stretch area. New

peaks appeared after modification in the alkane C–H stretch region, at 2850–2950 cm^{-1}, corresponding to the effect of HDTMA-Br as a cationic surfactant [15,32]. The functional group associated with the alkane C–C stretch was visible at peak absorption bands of 2852.62 and 2920.15 cm^{-1}, respectively, indicating a long-chain, linear aliphatic molecule.

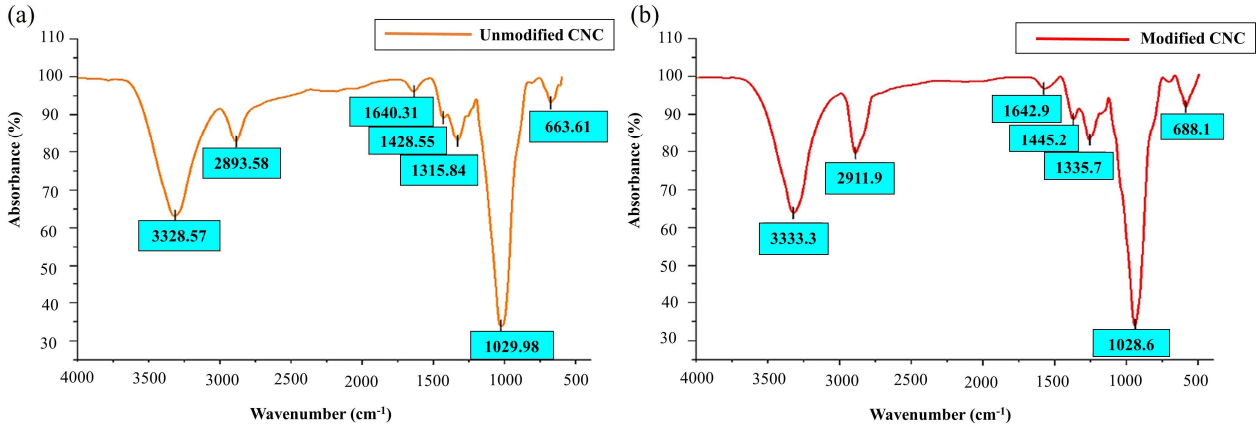

Figure 9. FTIR result for (a) unmodified CNC and (b) modified CNC.

3.2. TG-DTA analysis

The TG-DTA of unmodified and modified CNC was carefully discussed and analyzed, as shown in Figure 10a,b.

3.2.1. TG-DTA analysis for unmodified CNC

The thermograph of unmodified cellulose nanocrystals, as shown in Figure 10a, indicates that the initial weight loss during the drying stage, between 150 and 200 °C, is 3.172%, which can be attributed to the removal of possible moisture and volatile organic compounds. However, the total weight loss during the decomposition/degradation stage, subjected to temperatures ranging from 171 to 410 °C, is 63.946%.

At these temperatures, depolymerization events reduce the length of polysaccharide polymers from 1000 to 200 monomer units, resulting in mass loss. Furthermore, the total unstable weight loss after reaching the carbonization stage, at temperatures ranging from 410 to 700 °C, from the degradation stage is 27.69%, resulting in a total weight loss of 5.19%. Ultimately, the complete biodegradation of cellulose yields biomass, carbon dioxide, methane, and water under aerobic conditions and carbon dioxide and water under anaerobic conditions [35].

The unmodified CNC-powdered sample was subjected to differential thermal analysis on the same thermal analyzer for 4 min, with temperatures ranging from 30 to 900 °C. Figure 10a displays a high point where the CNC absorbed 3,401.38 mJ of heat energy at 94.68 °C. Furthermore, a high point of 50 to 100 mW heat absorption resulted in a considerable increase in thermal energy of 4,909.81 mJ. The increase in heat energy may result in the evaporation of more moisture in the sample as weight loss continues to climb.

3.2.2. TG-DTA analysis for modified CNC

The modified CNC-powdered sample was evaluated using a thermal analyzer, PerkinElmer STA 6000. The thermograph of modified cellulose nanocrystals, as shown in Figure 10b, indicates that the initial weight loss during the drying stage, between 150 and 200 °C, is 1.02%, which can be attributed to the removal of a small amount of moisture and volatile organic compounds.

However, the overall weight loss throughout the decomposition/degradation stage at 153–410 °C is 71.27%. This suggests that depolymerization events shorten the length of polysaccharide polymers, leading to mass loss. Furthermore, the coated HDTMA-Br surfactant causes more mass loss during the degradation stage of the modified CNC [32].

The modified CNC-powdered sample was subjected to differential thermal analysis using the same thermal analyzer for 4 min, with temperatures ranging from 30 to 900 °C. Figure 10b displays a peak where the CNC absorbed 3152.42 mJ of heat energy at 94.68 mW. Furthermore, a high peak point from 0 to 50 mW of heat absorbed resulted in a considerable increase in thermal energy of 3347.72 mJ. The coated structure of the HDTMA-Br surfactant adsorbed by CNC significantly contributed to a decrease in heat energy compared to unmodified CNC. Thus, modified CNCs emit less exothermic energy than unmodified CNCs [15,32–35].

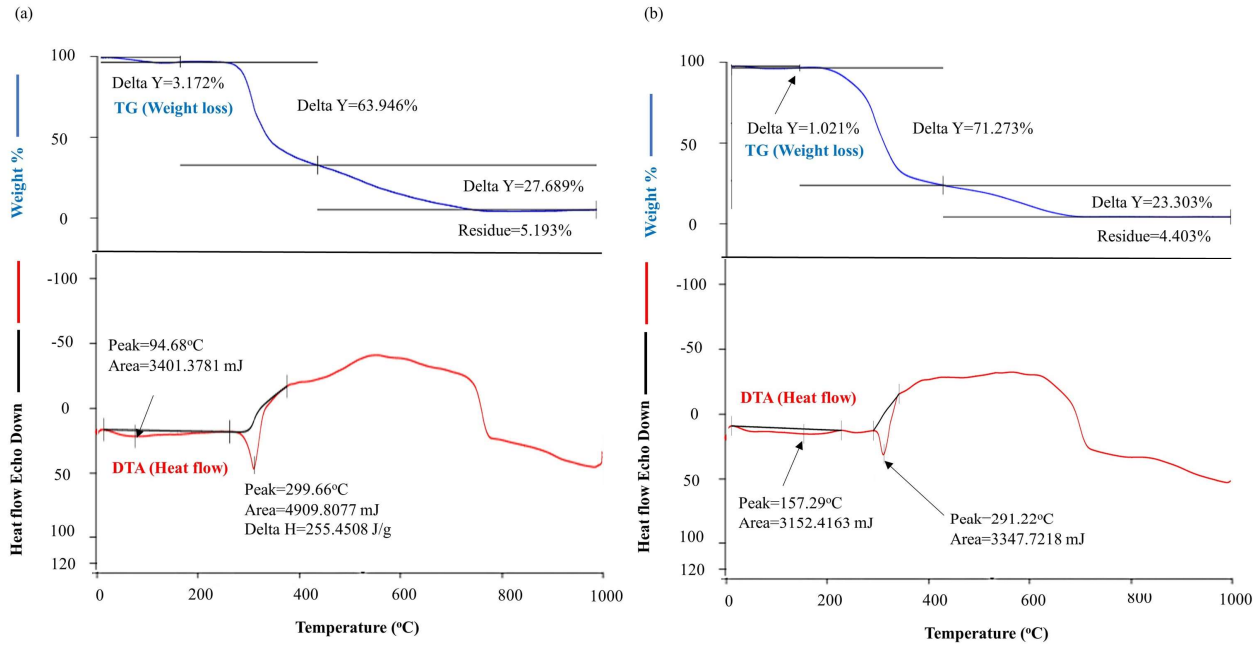

Figure 10. TG-DTA result for (a) unmodified CNC and (b) modified CNC.

3.3. DSC analysis

The DSC graph, as shown in Figure 11a,b, illustrates the thermal behavior of the 3D-printed composite PLA-TPU-CNC in both its unmodified and modified forms.

3.3.1. DSC result of 3D printed PLA-TPU with unmodified CNC

The glass transition (T_g), crystallization (T_c), and melting point (T_m) temperatures of PLA-TPU with unmodified CNC, as demonstrated in Figure 11a, were determined to be 61.24, 101.03, and 147.33 °C, respectively, which yielded slightly lower values than those of PLA-TPU with modified CNCDSC result of modified CNC.

3.3.2. DSC result of 3D printed PLA-TPU with modified CNC

The endothermic peaks of the composite with modified CNC exhibited a higher glass transition temperature (T_g) of 62.28 °C and a melting temperature of 148.5 °C, as shown in Figure 11b, compared to the composite with unmodified CNC. The absorbed energy of −183.25 mW for T_g and 305.61 mW for T_m demonstrated the contribution of modified CNC as an additive component to the PLA-TPU blend. The structure of modified CNC, resulting from the adsorption of the surface-active agent HDTMA-Br during surface modification, increased both the endothermic and exothermic reactions of the PLA-TPU blend [34,35].

Additionally, the composition of the soft segment in TPU can influence the crystallization temperature and the resulting crystal structure. Various factors, including the preparation method, heating process, and the addition of fillers, can influence the composite's crystallization behavior. Moreover, when the T_c value of TPU is lower, a higher percentage of Form-I crystals is produced. Thus, repeated melting and recrystallization can achieve a more intricate melting behavior during the melting of Form I. Likewise, the degree of interfacial adhesion bonding between the modified CNC and the matrix contributed significantly to the composite's thermal transition and stability. Furthermore, the slight increase in T_g under modified CNC shows an improvement in the rigidity of the composite's structure [32,34,35].

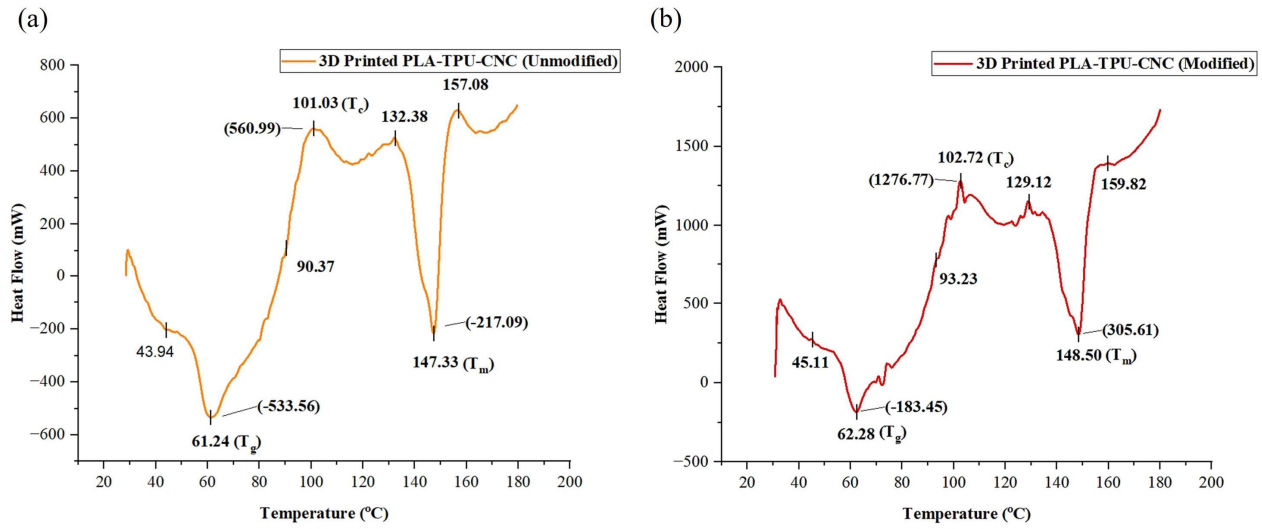

Figure 11. DSC result for (a) 3D printed PLA-TPU-CNC (unmodified) and (b) 3D printed PLA-TPU-CNC (modified).

3.4. XRD analysis

The crystallite structure of CNC is vital to its reinforcing effects. Figure 12a,b illustrate the X-ray measurements performed on both the unmodified and modified CNCs.

3.4.1. XRD analysis for unmodified CNC

The XRD pattern of unmodified CNC, with diffraction peaks at 16.02 and 22.48° corresponding to the (110) and (200) diffraction patterns, was noticeable in the graph, commonly exhibiting peaks characteristic of type I cellulose [35].

The crystallite structure of CNC is crucial in its reinforcing effects, and it should be preserved during modification to maintain these reinforcing effects. The crystallite structure was investigated using X-ray diffraction to assess the effect of modification [21].

3.4.2. XRD analysis for modified CNC

The modified CNC's X-ray diffraction pattern exhibited a typical X-ray diffraction pattern of cellulose type I, characterized by diffraction peaks at 16.6 and 22.76°, corresponding to the (110) and (200) planes of cellulose type I. Modifying CNC with HDTMA-Br under various conditions did not considerably change its X-ray patterns. However, a higher peak intensity was observed, indicating that the modified cellulose's crystalline structure had been improved [15,35]. This indicates that HDTMA-Br contributes more atoms in the CNC crystal region, resulting in a high degree of crystallinity. Thus, this type of cationic surfactant contributes to the structural changes in alignment that produce highly ordered crystals in cellulose [32].

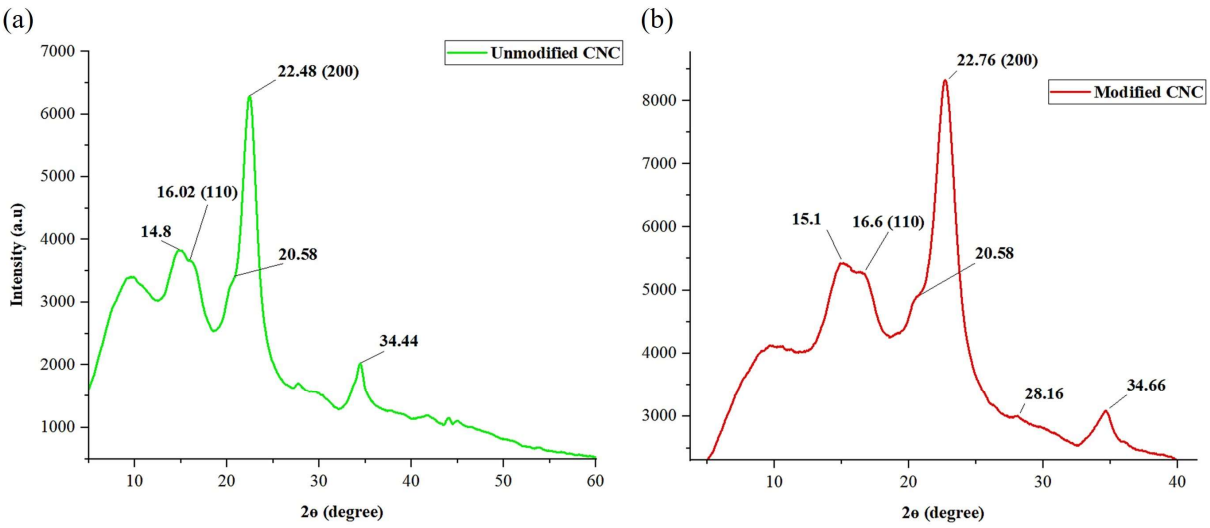

Figure 12. XRD result for (a) unmodified CNC and (b) modified CNC.

3.5. TEM analysis

As shown in Figure 13a,b, the TEM image of the unmodified CNC reveals the actual nanometric/sub-nanometric lateral resolution of the purchased spray-dried cellulose, with a scale

of 100–200 nm. The average width and diameter of CNC, as measured using TEM results and ImageJ software, are 6.30 and 125 nm, respectively, yielding an aspect ratio (L/d) of 19.

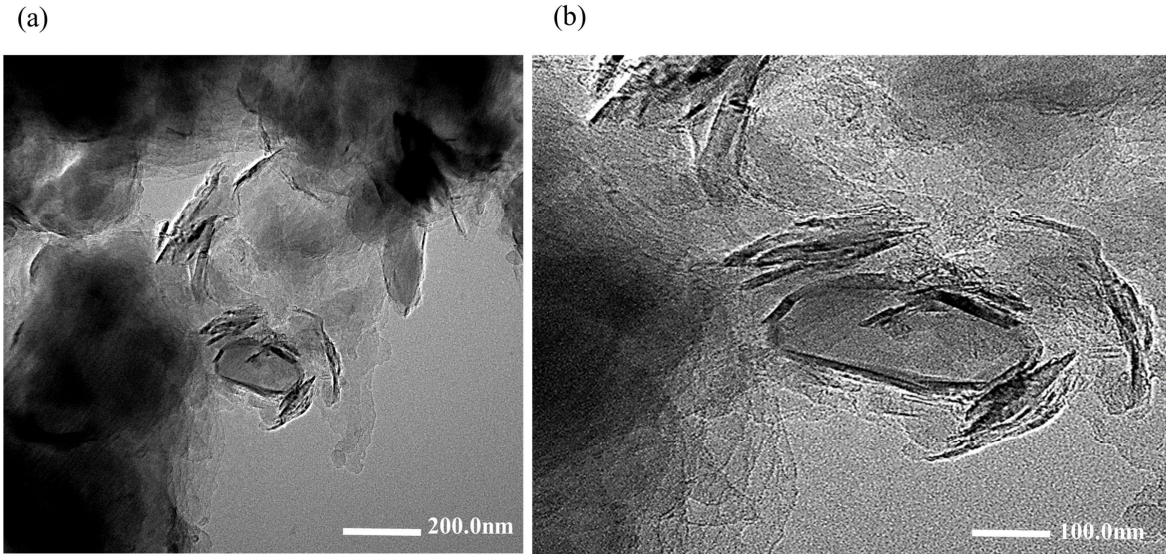

Figure 13. TEM image for unmodified CNC at a scale of (a) 200 nm, and (b) 100 nm.

3.5.1. TEM image of unmodified CNC

The particle size of the measured unmodified CNC is nearly similar to the specifications provided by the CNC supplier. The needle-like shape of the CNC structure has been proven to have an even and consistent distribution throughout the entire matrix structure [35,36].

The average width/diameter and length of the CNC, as measured from the TEM result using ImageJ software, are 2.86 and 147 nm, respectively. Likewise, the particle size of the measured CNC is improved compared to its original specifications.

3.5.2. TEM image of modified CNC

The TEM image of the modified CNC, as shown in Figure 14a,b, reveals the actual nanometric/sub-nanometric lateral resolution of the surface-treated spray-dried cellulose at a scale of 100–200 nm, providing a clear view of a more crystalline structure compared to the unmodified one.

In addition, the surface of the modified CNC was significantly enhanced due to the effective interaction of the cationic components of HDTMA-Br with its crystallite structure, resulting in a more organized crystal arrangement [32,35]. The modified CNC structure's needle-like shape provided excellent and more consistent particle dispersion throughout the entire matrix structure than the unmodified one [35,36].

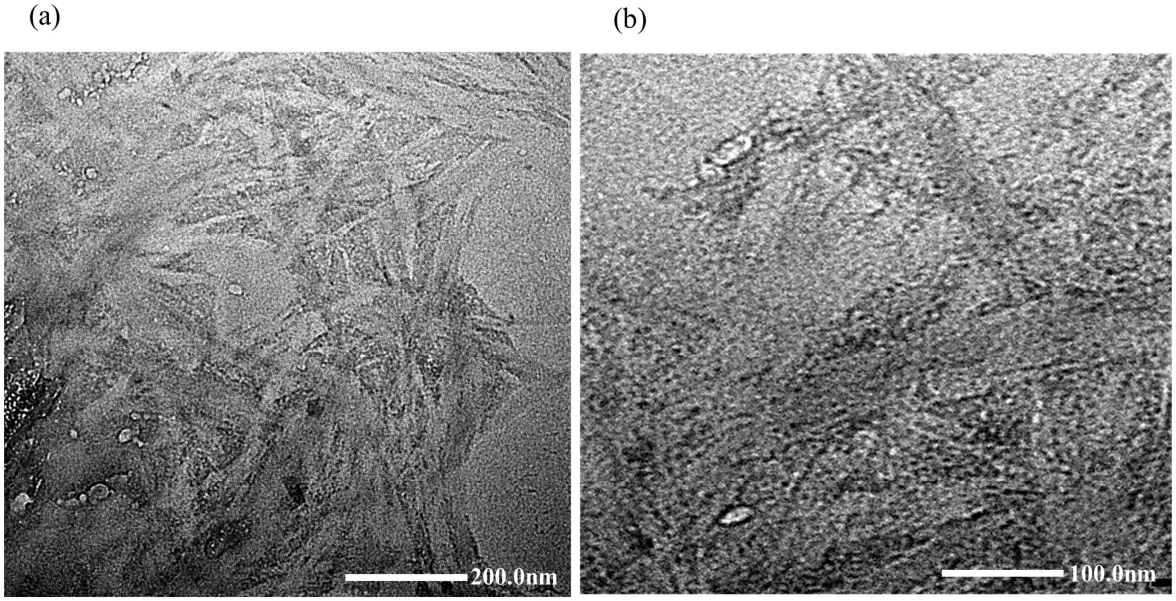

Figure 14. TEM image for modified CNC at a scale of (a) 200 nm, and (b) 100 nm.

3.6. SEM-EDX analysis

Figures 15–19 illustrate the outcomes of the usual SEM and EDX analysis of PLA, TPU, and CNC raw materials.

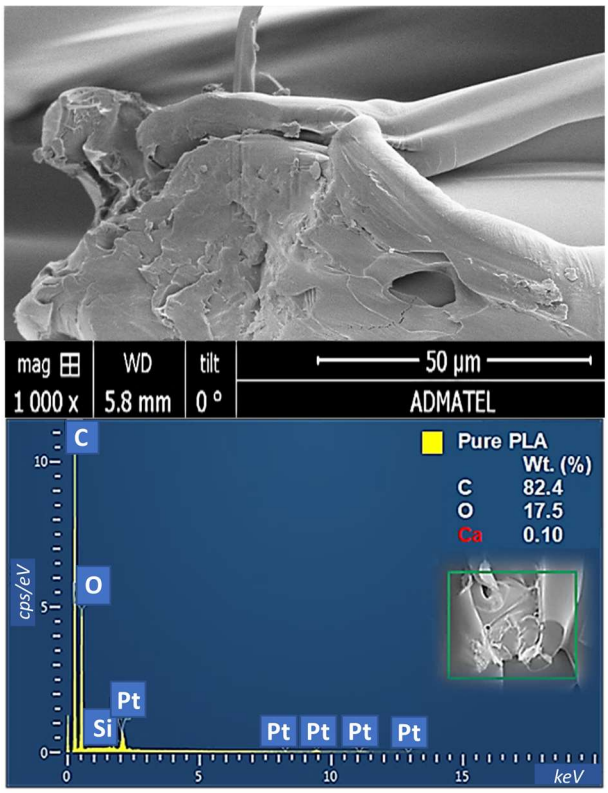

Figure 15. SEM-EDX result for PLA.

Expressed as a weight percentage (wt%), the EDX spectra of pure PLA typically display peaks for carbon and oxygen, as shown in Figure 15, with peak values of 82.4 wt% for carbon and 17.5 wt% for oxygen. The EDX spectra of pure TPU typically display peaks for carbon, nitrogen, and oxygen, as illustrated in Figure 16, yielding peak values of 69.7 wt% for carbon, 23.0 wt% for nitrogen, and 0.277 wt% for oxygen.

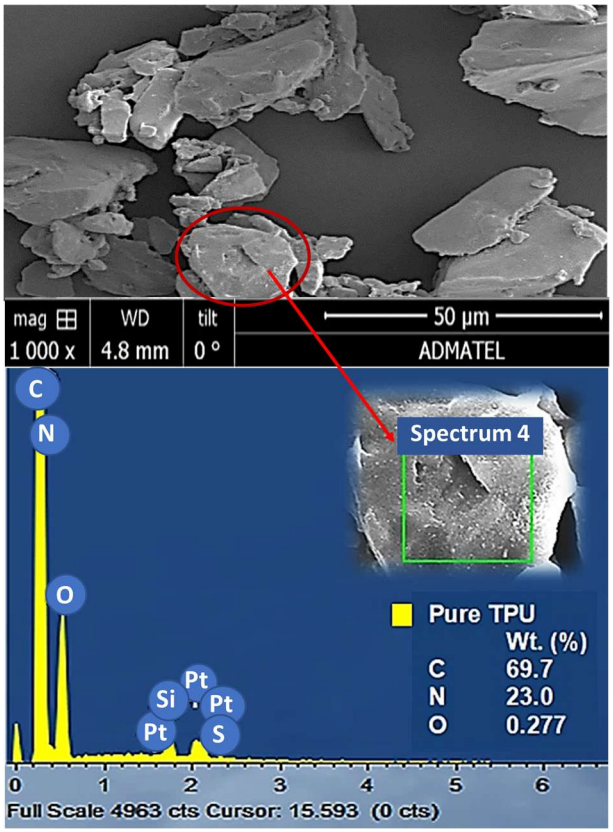

Figure 16. SEM-EDX result for TPU.

3.6.1. SEM-EDX image of unmodified CNC

The EDX spectra of the unmodified CNC demonstrate peaks for carbon and oxygen, as illustrated in Figure 17. The unmodified CNC has a peak C value of 55.96 wt% and an O value of 43.3 wt%. The oxygen content of unmodified cellulose increases due to its natural hydrophilicity compared to hydrophobic surface-treated cellulose [35].

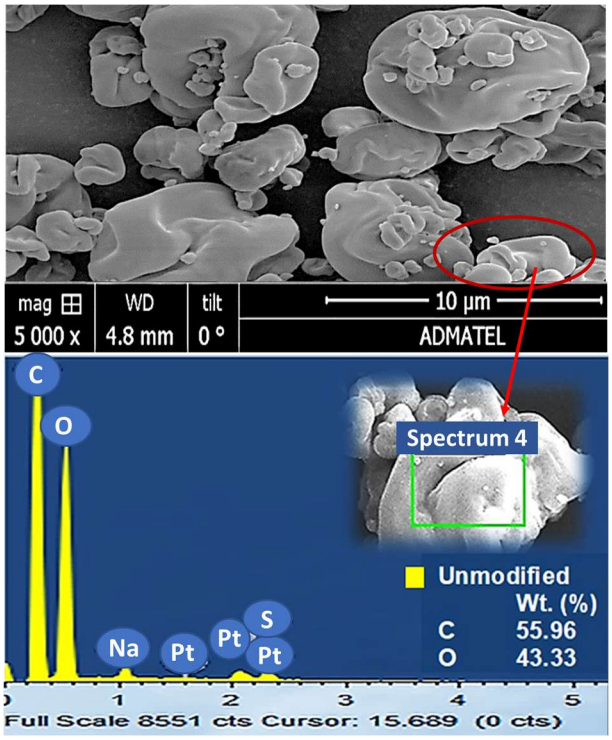

Figure 17. SEM-EDX result for CNC (unmodified).

3.6.2. SEM-EDX image of modified CNC

The SEM-EDX results in Figure 18 show a significant change in the surface texture of the modified CNC. HDTMA's active participation as a cationic surfactant on the surface of unmodified CNC produces an adequate coating and interaction, potentially leading to compatibility with the hydrophobic matrix [15,32,34,35]. The modified CNC's EDX spectra in Figure 18 generated peaks for carbon, oxygen, and nitrogen. It has a peak C value of 61.2 wt%, an O value of 33.8 wt%, and an N value of 3.42 wt%.

The presence of nitrogen in the structure suggests that HDTMA-Br contributes some nitrogen atoms during CNC surface treatment. Moreover, Figure 19 demonstrates the smoothness of the PLA-TPU sample manufactured using 3D printing. Additionally, Figure 20 illustrates the interfacial adhesion of CNC to the smooth surface of the 3D-printed PLA-TPU.

However, some voids were observed within the 3D-printed section of the specimen due to inconsistencies and instability that may have occurred during the 3D printing process [3,30,31,37]. It was also observed that variations in filament diameter size caused inconsistencies during the extrusion process. Moreover, CNC's hydrophilic property could also be a potential agglomeration factor affecting its dispersion within the PLA-TPU matrix [32–34].

The EDX spectra of the manufactured PLA-TPU typically display peaks for carbon and oxygen, as illustrated in Figure 19. The 3D-printed PLA-TPU has a peak C value of 61.0 wt% and an O value of 38.9 wt%.

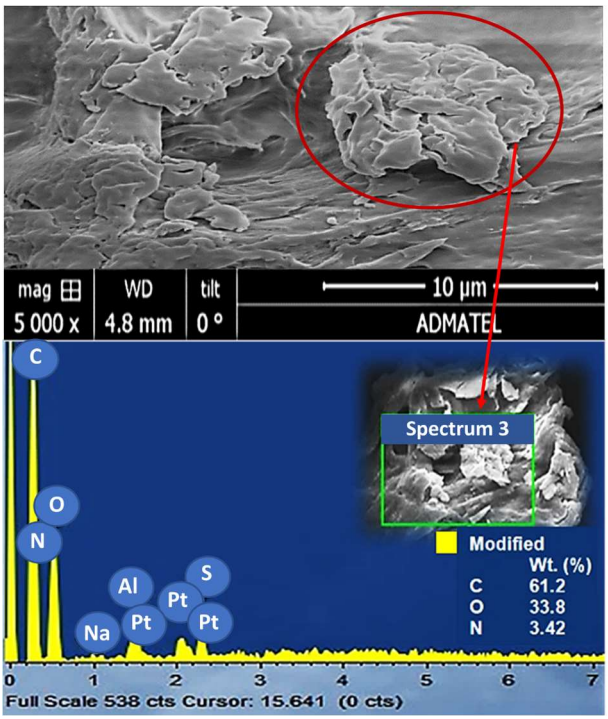

Figure 18. SEM-EDX result for CNC (modified).

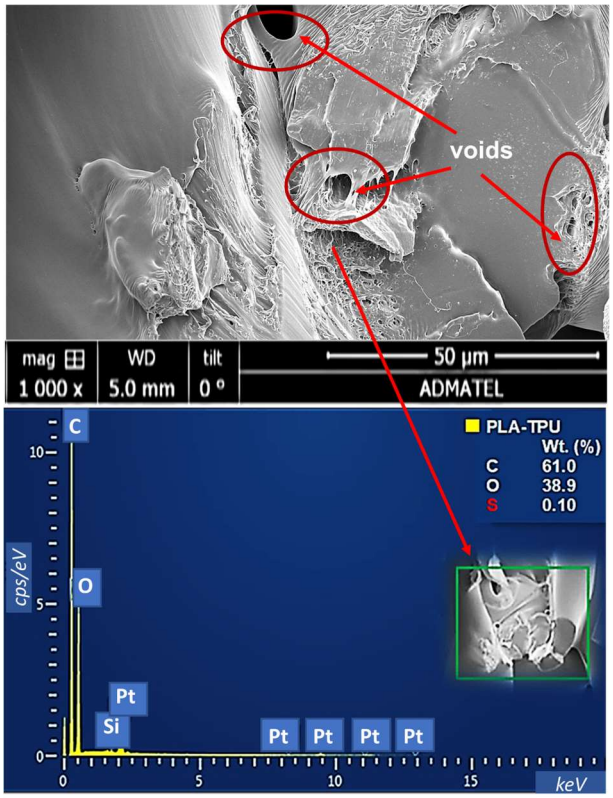

Figure 19. SEM-EDX result for 3D printed PLA-TPU.

3.6.3. SEM-EDX image of 3D-printed PLA-TPU with unmodified CNC

The EDX spectra of the manufactured composite nanostructure typically display peaks for carbon and oxygen, which are also present in both the unmodified and modified CNC [35], as illustrated in Figures 20 and 21. The unmodified CNC 3D-printed composite has a peak C value of 63.6 wt% and an O value of 36.1 wt%.

Despite the smooth 3D printing process, voids remain on some surface regions of the 3D-printed PLA-TPU and PLA-TPU [37] with unmodified CNC, increasing the specimen's porosity. Variations in filament diameter cause the melted material to be extruded unevenly throughout the extrusion process. This may result in blockage of melted material before it exits the nozzle due to partial melting [3,30], as noted by Rahmatabadi et al.

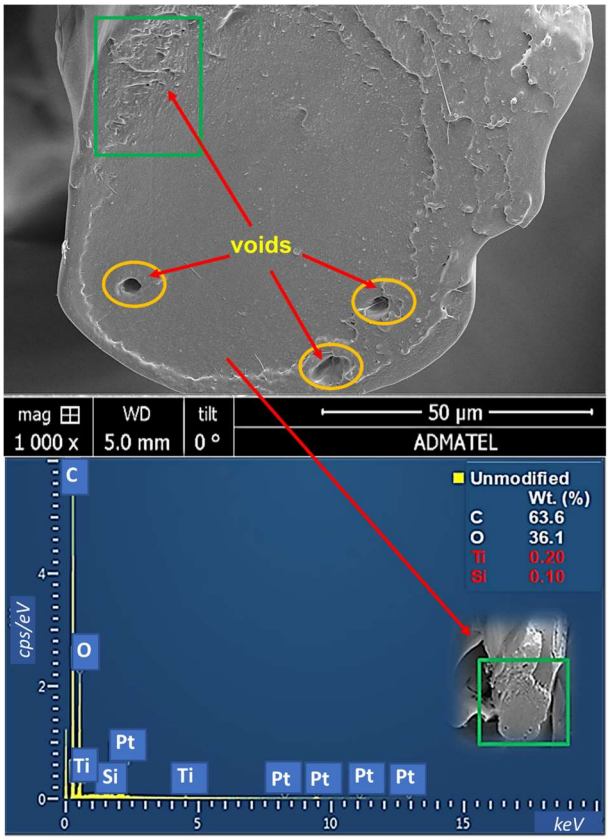

Figure 20. SEM-EDX result for 3D printed PLA-TPU-CNC (unmodified).

Furthermore, to resolve this issue, another set of composite filaments was prepared before the 3D printing process, where the actual RPM range during filament extrusion via a single-screw filament maker is adjusted to 5.50 ± 1 instead of 5.50 ± 3 RPM until the diameter size of the extruded filament is obtained and consistent at 1.65 to 1.85 mm, thus a 1.75 mm diameter size is preferred. Moreover, the inconsistencies produced by CNC's hydrophilic behavior may be a potential source of the agglomeration factor impacting its dispersion within the PLA-TPU matrix, resulting in uneven printing of each surface layer [3,32–34].

3.6.4. SEM-EDX image of 3D-printed PLA-TPU with modified CNC

Furthermore, the peak C value for 3D-printed composites using modified CNC is 64.0 wt%, while the peak O value is 35.8 wt%. Although a possible agglomeration may occur during dispersion, it was observed that each group of CNC could be seen (as tiny white dots), indicating that most of the portion on the surface reveals good dispersibility of the CNC in the polymer, but not as much as the modified one. We found that HDTMA-Br can transform CNC from a hydrophilic nanoparticle to a hydrophobic nanoparticle [15,32–35]. The dispersion of modified CNC (tiny white dots inside the triangle) was observed on the composite's smooth surface, as shown in Figure 21.

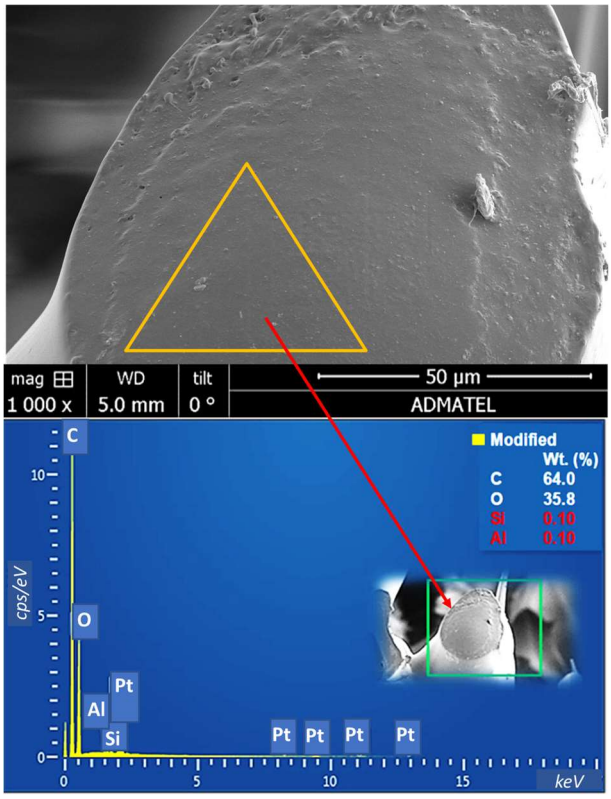

Figure 21. SEM-EDX result for 3D printed PLA-TPU-CNC (modified).

Moreover, surfactants can enhance the dispersibility of CNC nanoparticles, and drug carriers made of CNC/surfactant complexes have potential. Nevertheless, surfactant modification of CNC shows promise, as mentioned by Kaboorani et al.

The commercialization of this approach is highly dependent on HDTMA's low toxicity and rapid reaction time, which are two significant advantages. Adjusting the HDTMA-Br concentration is one way to regulate hydrophobicity [15].

The reaction's duration primarily affected the surface change. Depending on the type of polymer being mixed, CNC should adjust the hydrophobicity to a reasonable level. If the polymer in question is exceptionally hydrophobic, CNC requires a high concentration of HDTMA-Br.

Other suggested methods do not offer the advantages of modifying CNC with HDTMA-Br. The carbon content increases when HDTMA-Br is combined with cellulose nanocrystals in a 3D-printed

composite structure. Due to surface modification, the oxygen content of CNC reduces as its hydrophobicity rises [32,33].

3.7. AFM analysis

Researchers have studied the surface topology of PLA-TPU and PLA-TPU with modified and unmodified CNCs to further investigate the interfacial adhesion behavior of CNCs within the PLA-TPU polymer matrix.

As presented in Figure 22a,b, the average surface roughness of PLA-TPU (80:20) was 75.015 nm, increasing to 75.939 nm at 150.594 nm Ra shortly after specimen failure. The topographic image reveals slight surface roughness before and after mechanical performance, attributed to the crystalline structures of the PLA-TPU matrix.

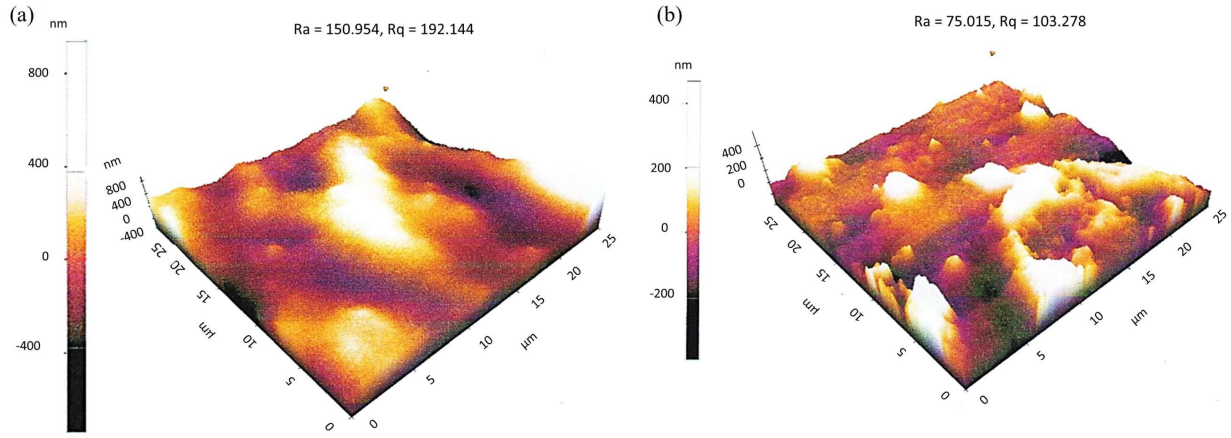

Figure 22. AFM image of 3D printed PLA-TPU. (a) Before mechanical testing and (b) after mechanical testing.

3.7.1. AFM image of 3D-printed PLA-TPU with unmodified CNC

Additionally, in Figure 23a, PLA-TPU with unmodified CNC before mechanical testing exhibited a 79.77 nm decrease in surface roughness compared to PLA-TPU-CNC after mechanical testing, as shown in Figure 23b. This increases the surface area and creates an adhesive bond between the CNC and the polymer. After mechanical testing, the topographic image of PLA-TPU-CNC reveals a significant improvement in mechanical performance both before and after testing.

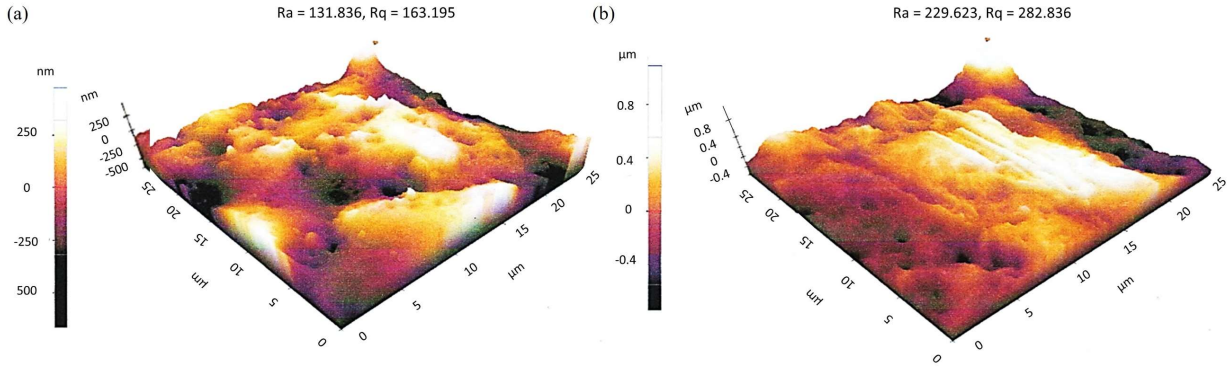

Figure 23. AFM image of 3D printed PLA-TPU-CNC (unmodified). (a) Before mechanical testing and (b) after mechanical testing.

3.7.2. AFM image of 3D-printed PLA-TPU with modified CNC

Furthermore, only a few brighter images were detected in the composite sample with modified CNC, as shown in Figure 24a,b. These are likely similar to the topographic image of PLA-TPU in Figure 22a,b. This indicates that the structural component of the unmodified CNC in Figure 23a,b protrudes on the surface, contributing to the composite's overall surface roughness.

Immediately after mechanical testing, the average surface roughness (Ra) of PLA-TPU-CNC increased significantly to 78.207 nm due to the successful adhesion of modified CNC within the polymer matrix. The topographic image of PLA-TPU with modified CNC, both before and after mechanical testing, revealed a slight decline in surface roughness compared to the composite with unmodified CNC. This can be attributed to the modified CNC's compatibility with PLA-TPU, which enables the smoothing of the structure's surface [15,35].

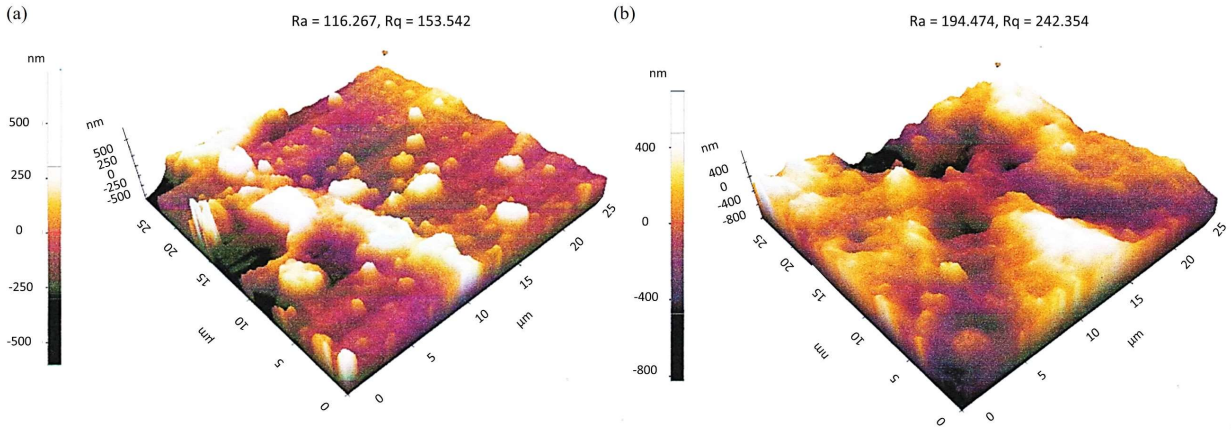

Figure 24. AFM image of 3D printed PLA-TPU-CNC (modified). (a) Before mechanical testing and (b) after mechanical testing.

The constant rise in surface roughness of all composite samples, as shown in Figure 25, indicates a significant increase in surface area resulting from the application of particular forces within the composite's structure. Although the surface area increases, protrusions of CNC particles attached to the surface and their uneven impact are relevant to the structural component of the remaining composite specimens.

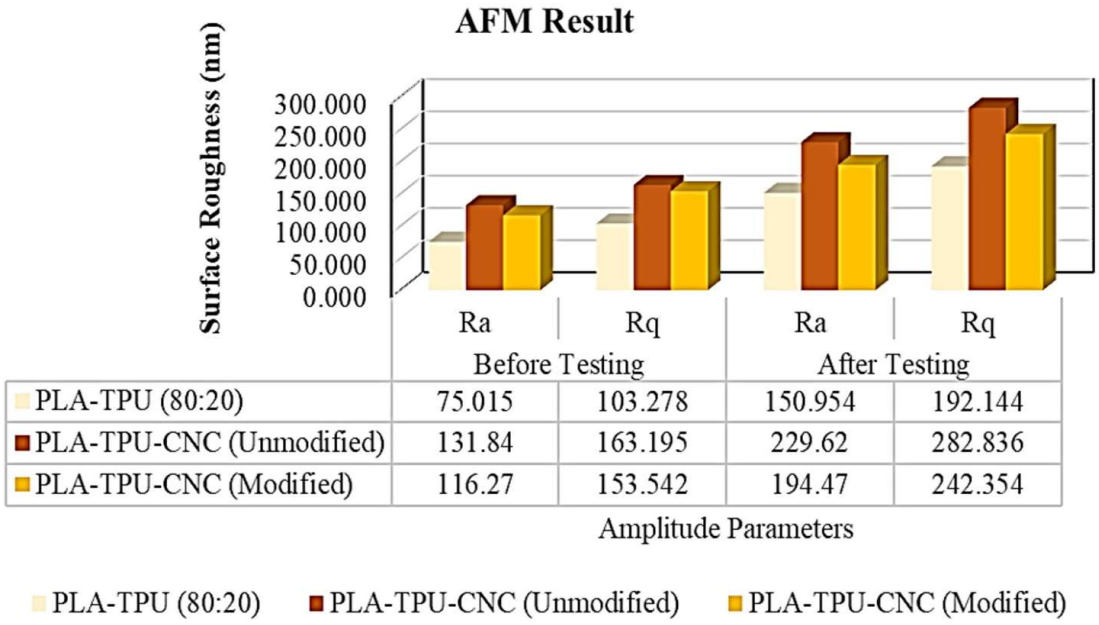

Figure 25. AFM result before and after mechanical testing.

3.8. Tensile test

The tensile properties of the PLA, PLA-TPU, and PLA-TPU-CNC (both unmodified and modified) samples were calculated as the average of five specimens, as per ASTM D638 [38]. As shown in Figure 26a, PLA-TPU (80:20) has achieved the highest average tensile strength of 17.94 MPa among the other formulations, representing a 23.47% increase over the composite with 3% unmodified CNC concentrations, which has the highest tensile strength value among the other unmodified CNC variations.

3.8.1. Tensile test result for PLA-TPU with unmodified CNC

Furthermore, the composite with 0.05% unmodified CNC obtained a 44.8% decrease in tensile strength compared to the PLA-TPU blend. Also, the composite with 1% unmodified CNC experienced a 58.5% decrease. Nevertheless, PLA-TPU with a 3% unmodified CNC concentration showed a significant improvement in tensile strength of approximately 17%–28% compared to the other variations at 0.05% and 1% concentrations, despite a decrease of 23.5% compared to the PLA-TPU blend. One likely reason for this is the ineffectiveness of integrating unmodified CNC into PLA-TPU blends, as well as the poor quality of the 3D printing process. Further investigation and analysis are needed to enhance the structure of the 3D-printed composite.

3.8.2. Tensile test result for PLA-TPU with modified CNC

The tensile strength of PLA-TPU at 0.05% modified CNC, as shown in Figure 26b, provides the highest strength among all other types of materials, including PLA, TPU, PLA-TPU, and the other CNC concentrations tested. Compared to composites at 1% and 3% modified CNC concentrations, the tensile strength of the 0.05% sample increased by 15.5% and 49.1%, respectively.

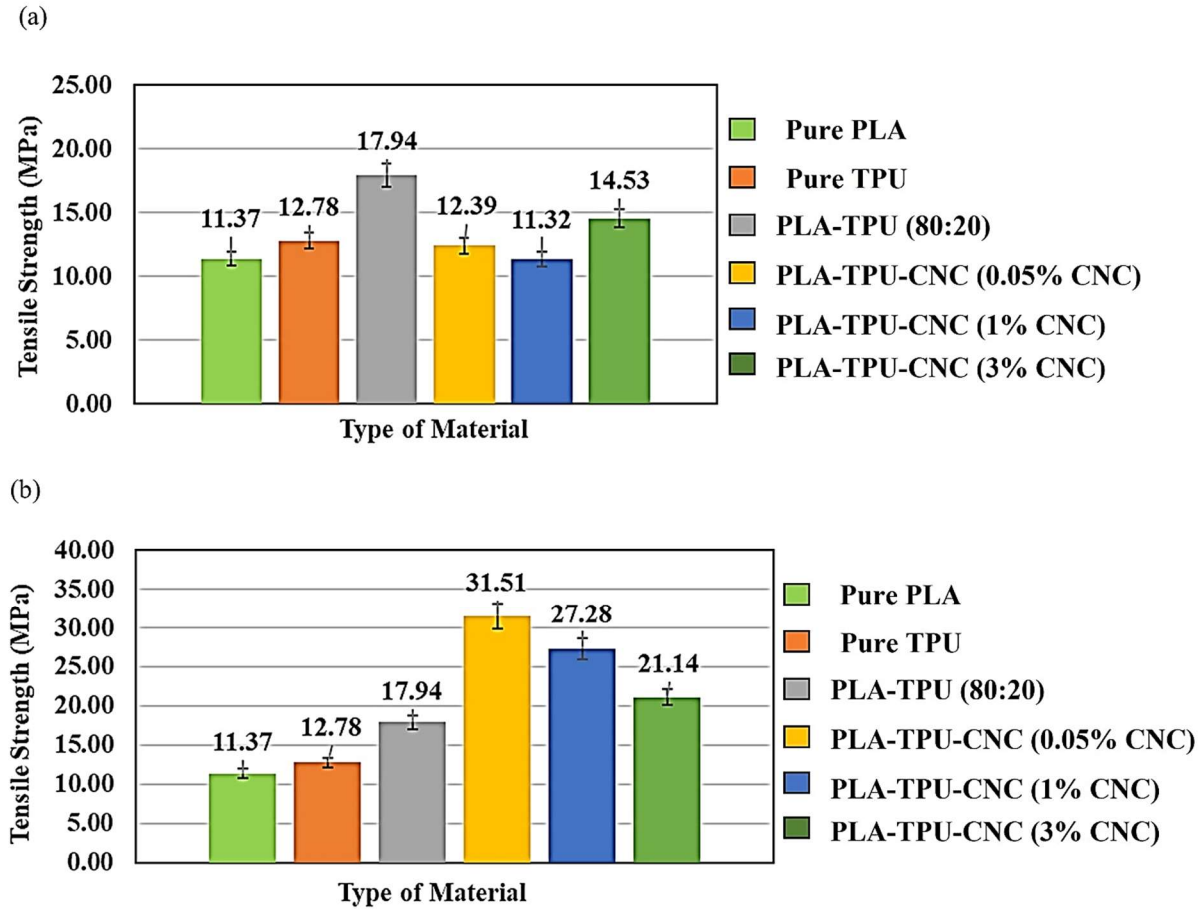

Figure 26. Tensile test results for PLA-TPU with (a) unmodified CNC and (b) modified CNC.

The composite with modified CNC at a 0.05% concentration exhibits a significantly higher tensile strength of 19.12 MPa than the composite with unmodified CNC at the same 0.05% concentration. The composite with 1% modified CNC improved dramatically by 141% compared with the 1% unmodified CNC composite. A similar trend was observed with the composite at 3% modified CNC, resulting in a 45.5% increase over the composite with 3% unmodified CNC. When CNC is treated with a cationic surfactant (hexadecyltrimethylammonium bromide), the interfacial bonding between the hydrophilic CNC and the hydrophobic PLA-TPU (80:20) is significantly improved compared to the interaction of unmodified CNC with both thermoplastic matrices [21,32,35].

During the 3D printing process, it was discovered that the smooth release of extruded PLA-TPU filament significantly contributes to the finest and most balanced distribution of melted filament materials throughout the entire 3D printing process [30,31,37], as illustrated in Figure 27a. The default 3D-printing parameters, such as infill density, infill pattern, raster width, layer height, and perimeter, when combined with extrusion speed, nozzle temperature, and build plate temperature, produce a specimen design that meets the ASTM D638 standard.

However, in most cases, for the 3D printing of composite materials that are typically reinforced with CNC or fibers, imperfections such as incomplete infill patterns and density issues due to insufficient extruded filament material passing through the nozzle cannot be avoided, as shown in Figure 27b.

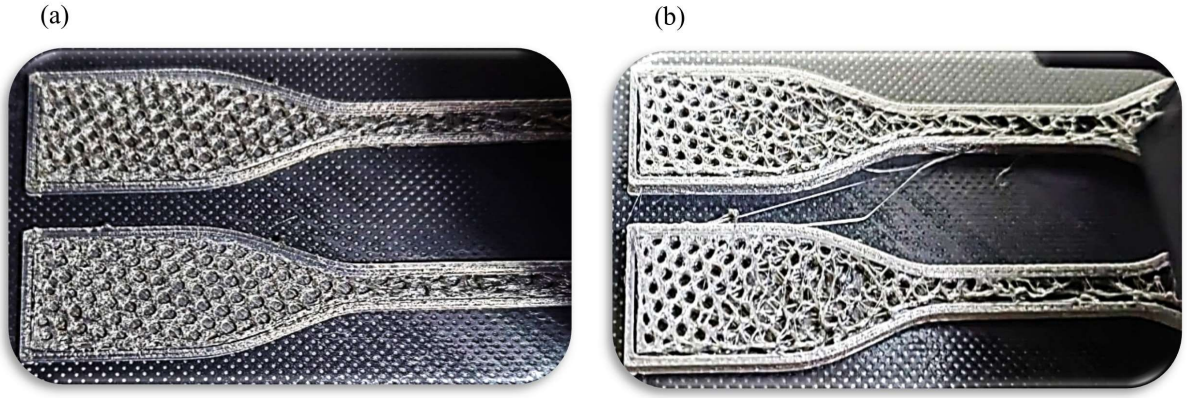

Figure 27. 3D printing process result: (a) smooth printing process, and (b) imperfect 3D printing process.

Moreover, the presence of voids, as seen in Figure 20, could be considered a factor influencing the composite's mechanical performance [3]. The 3D-printed structure of the specimen in Figure 27b demonstrates the condition of under-extrusion and blockage caused by a part of the filament that is either too small or oversized in diameter [17].

Statistical analysis for each type of mechanical properties via the use of analysis of variance (ANOVA) covered different sources of variations which includes but not limited to: SS—sum of squares; df—degrees of freedom; MS—mean square; F—ratio between-group and within-group variance; P-value (probability value); F crit—random variable threshold. The F-statistics for all concentration levels in Table 2 showed a significant ratio of 23.45, surpassing the F-critical value of 2.21. Moreover, the p-value obtained is ≤0.05, indicating that the design criteria between each group or level of concentration are statistically significant.

Table 2. One-way ANOVA: tensile test (MPa).

Summary						
Groups	Count	Sum	Average	Variance		
Pure PLA	5	56.8700	11.37400	1.96996		
Pure TPU	5	64.5873	12.91746	0.40742		
PLA-TPU	5	89.7263	17.94526	11.98783		
Unmodified CNC 0.05%	5	61.9501	12.39002	3.06368		
Unmodified CNC 1%	5	56.5964	11.31927	4.49836		
Unmodified CNC 3%	5	72.6745	14.53489	17.19633		
Modified CNC 0.05%	5	157.5601	31.51202	0.696114		
Modified CNC 1%	5	136.4205	27.28410	4.674663		
Modified CNC 3%	5	105.6781	21.13562	60.14377		
ANOVA						
Source of variation	SS	df	MS	F	P-value	F crit
Between groups	2180.8570	8	272.607	23.447	4.286E-12	2.2085
Within groups	418.5525	36	11.6264			
Total	2599.409437	44				

3.9. Flexural test

The flexural strength of the various samples was determined using a three-point bending test, as specified in ASTM D790 [39]. Figure 28a,b show the values obtained and projected based on an average of five specimens.

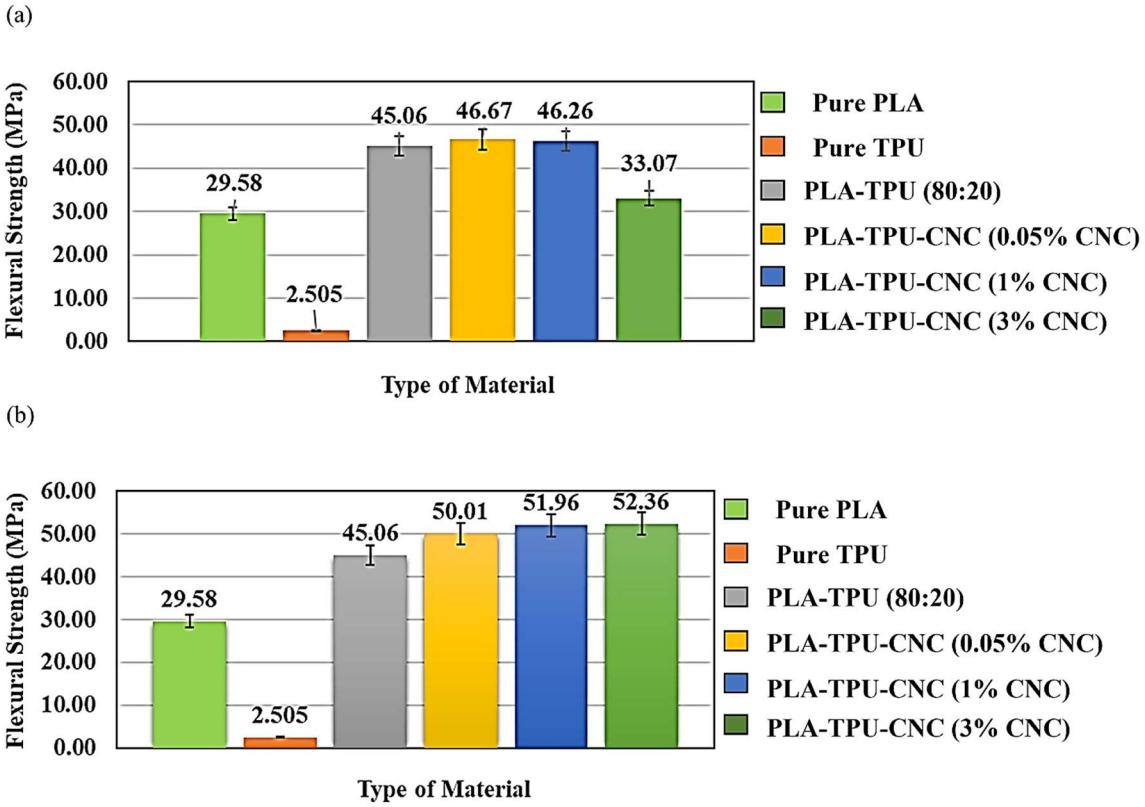

Figure 28. Flexural test results for PLA-TPU with (a) unmodified CNC and (b) modified CNC.

3.9.1. Flexural test result for PLA-TPU with unmodified CNC

As shown in Figure 28a, PLA-TPU with 0.05% unmodified CNC had the highest flexural strength of all the materials tested, with a value of 46.67 MPa. Furthermore, this composite shows no significant difference compared to PLA-TPU (80:20) and PLA-TPU-CNC (1%).

However, when compared individually to pure PLA, TPU, and PLA-TPU-CNC (3%), this composite exhibits significantly improved flexural performance. The flexural performance of PLA-TPU (80:20) and PLA-TPU with unmodified CNC at 0.05% and 1% can be attributed to the stable extrusion of the filament, resulting from the smooth flow of the melted material during the 3D printing process. Nevertheless, in some circumstances with a more significant proportion of reinforced cellulose nanomaterial, such as in the case of a composite with 3% unmodified CNC, agglomeration may occur due to the hydrophilic properties of the reinforcing material, which affect its compatibility with the polymeric matrix [3].

3.9.2. Flexural test result for PLA-TPU with modified CNC

Similarly, all concentration levels (0.05%, 1%, and 3%) under this enhanced CNC demonstrated considerably higher flexural performance than all levels in the unmodified CNC group. Nonetheless, in Figure 28b, the composite with 0.05% CNC contributes an 11% to 69.1% increase compared with pure PLA and PLA-TPU blend. Moreover, a 7.16% rise was observed for the composite with 0.05% CNC compared with the unmodified 0.05% CNC. The composite with 1% CNC also demonstrates a terrific increase of 12.32% compared with the composite at 1% unmodified CNC.

Furthermore, PLA-TPU with modified CNC at 3% had the highest flexural strength of all tested materials, measuring 52.36 MPa. Although its flexural strength varied slightly from the other concentration levels in its group, this 3% modified CNC concentration achieves an impressive 58.3% improvement in flexural strength compared to a composite with 3% unmodified CNC.

The following figures demonstrate the capabilities of surface modification made to CNC using a cationic surface-active agent, HDTMA-Br. CNC's surface is highly responsive and functionalized due to its enormous surface area-to-volume ratio. Due to its chemical reaction with HDTMA-Br, the surface of CNC produced novel chemical groups, such as CH_2, CH_3, and quaternary ammonium cation groups, as shown in Figure 29a,b.

HDTMA-Br is a tetrasubstituted ammonium amphiphilic surfactant with a hydrophilic head and a hydrophobic tail, along with a long, straight alkyl chain. This makes it more compatible with hydrophobic PLA and TPU polymers [33].

It is readily available and inexpensive, offering advantages over other materials that modify CNC surfaces. As is the case with most cellulose derivatizations, the primary reactive sites for modifying cellulose's surface are its hydroxyl groups.

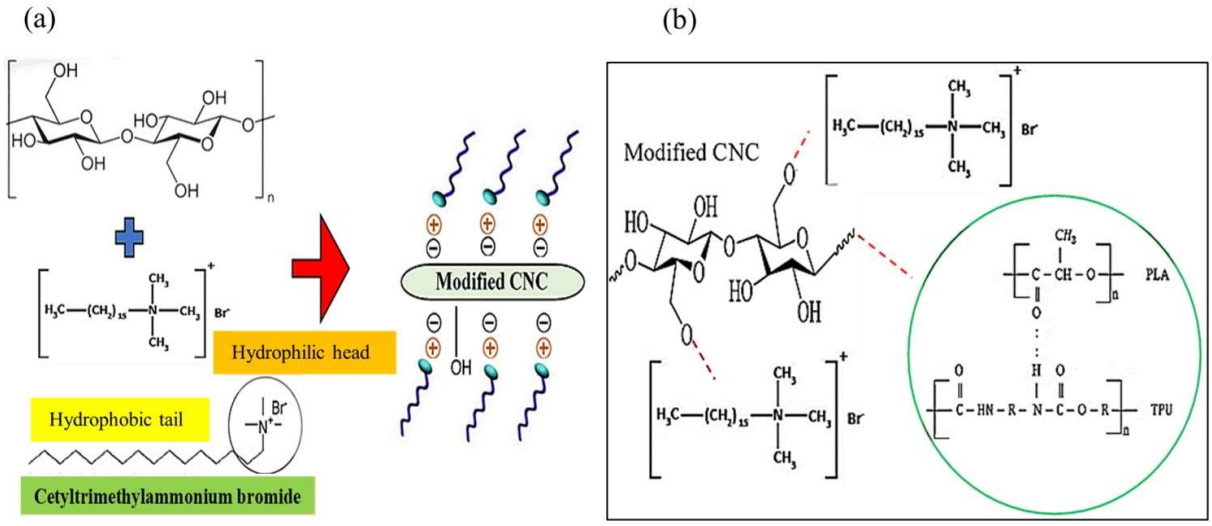

Figure 29. (a) Schematic molecular structure of modified CNC via surface treatment, and (b) molecular structure of PLA, and TPU.

Incorporating cationic surfactants, such as HDTMA-Br, enhances CNC's interfacial adhesion capabilities, yielding excellent compatibility and interactions with the polymer matrix's hydrophobic properties. To achieve the highest level of compatibility between the polymer and CNC, the hydrophobicity of CNC must be managed [15,32,33].

Table 3. One-way ANOVA: flexural test (MPa).

Summary						
Groups	Count	Sum	Average	Variance		
Pure PLA	5	147.8980	29.5796	12.93430		
Pure TPU	5	12.52457	2.50491	0.007546		
PLA-TPU	5	225.3200	45.0640	59.83703		
Unmodified CNC 0.05%	5	233.3484	46.6697	33.50994		
Unmodified CNC 1%	5	231.2982	46.2596	11.19137		
Unmodified CNC 3%	5	165.3306	33.0661	74.76028		
Modified CNC 0.05%	5	250.0575	50.0115	70.81660		
Modified CNC 1%	5	259.7801	51.9560	3.066146		
Modified CNC 3%	5	261.8224	52.3645	16.33807		
ANOVA						
Source of variation	SS	df	MS	F	P-value	F crit
Between groups	10336.0288	8	1292.004	41.167	7.607E-16	2.2085
Within groups	1129.8452	36	31.385			
Total	11465.8740	44				

The F-statistics for all concentration levels in Table 3 yielded a significant ratio of 41.17, surpassing the F-critical value of 2.21. Moreover, the p-value obtained is ≤0.05, indicating that the design criteria between each group or level of concentration are statistically significant.

3.10. Izod impact test

The Izod impact strength of the samples tested in the study, as per ASTM D256 [40], was evaluated using a Zwick/Roell HIT5.5P pendulum hammer with a 1J capacity. Figure 30a,b illustrate the impact strength values obtained by averaging the results of five specimens.

3.10.1. Izod impact test result for PLA-TPU with unmodified CNC

As shown in Figure 30a, the composite with 0.05% modified CNC exhibits an increase ranging from 17.6% to 149% compared with pure PLA, and PLA-TPU obtains an average value of 28.46 J/m.

PLA-TPU at 1% unmodified CNC exhibits the highest impact strength of all tested materials, measuring 34.80 J/m. Furthermore, compared to PLA-TPU and PLA-TPU-CNC at 0.05% and 3% under unmodified CNC, this composite showed a dramatic increase in impact strength, ranging from 22.3% to 43.8%. The composite at 3% unmodified CNC exhibited a slight increase in impact strength of 0.38 J/m with the PLA-TPU blend, but showed a significantly higher increase of 13.1 J/m compared with pure PLA.

3.10.2. Izod impact test result for PLA-TPU with modified CNC

Nevertheless, in Figure 30b, the composite with 0.05% modified CNC exhibits a significant increase of 71.5% compared with the composite at 0.05% unmodified CNC, which averages 48.41 J/m. Moreover, PLA-TPU-CNC, which was modified with 1% CNC, had the highest impact strength of all the tested materials, averaging 63.43 J/m. This concentration increases impact strength from 29.9% to 140.9% compared to the other concentrations of 0.05% and 3%, respectively. The 3% modified CNC composite exhibits a 7.12% higher impact strength than the 3% unmodified CNC, owing to enhanced cohesive adhesion between the modified CNC and the blended PLA-TPU. The prepared filament composite with modified CNC has achieved the desired diameter size and meets the requirements of a standard commercial filament.

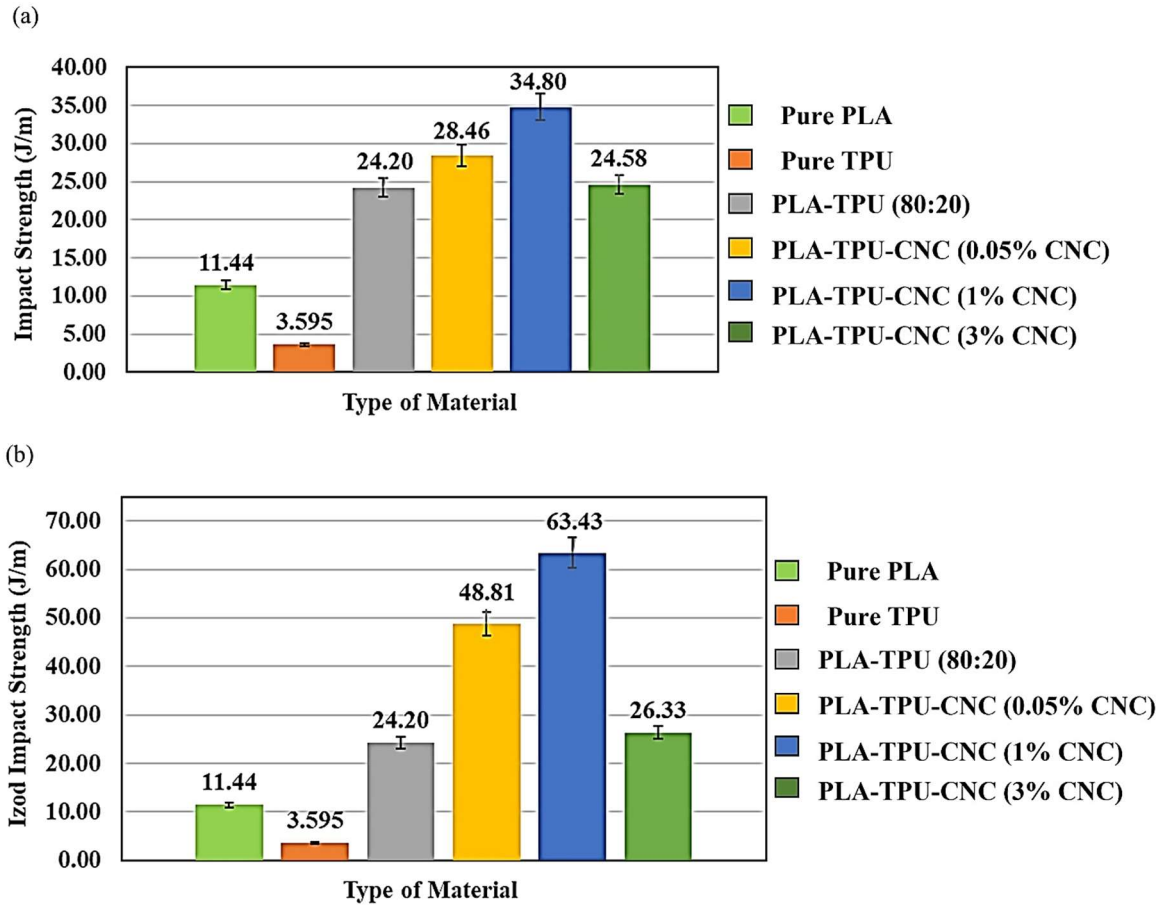

Figure 30. Izod impact test results for PLA-TPU with (a) unmodified CNC, and (b) modified CNC.

Furthermore, all concentration levels (0.05%, 1%, and 3%) under the modified CNC group exhibit a more significant impact than those under the unmodified CNC group. The interfacial adhesion of modified CNC to the hydrophobic nature of PLA-TPU leads to an absolute enhancement to the mechanical performance of the modified PLA-TPU CNC [1–3,6,7,21,32,35]. The F-statistics for all concentration levels in Table 4 yielded a significant ratio of 40.61, surpassing the F-critical value of 2.21. Moreover, the p-value obtained is ≤0.05, indicating that the design criteria between each group or level of concentration are statistically significant.

Table 4. One-way ANOVA: Izod impact test (J/m).

Summary						
Groups	Count	Sum	Average	Variance		
Pure PLA	5	57.19347	11.43869	4.02267		
Pure TPU	5	17.97594	3.595187	1.71968		
PLA-TPU	5	121.0088	24.20175	124.048		
Unmodified CNC 0.05%	5	142.3156	28.46311	41.9895		
Unmodified CNC 1%	5	173.9975	34.79949	64.1912		
Unmodified CNC 3%	5	122.8918	24.57835	22.5187		
Modified CNC 0.05%	5	244.0737	48.81475	8.53917		
Modified CNC 1%	5	317.1607	63.43214	90.3796		
Modified CNC 3%	5	131.6639	26.33278	4.57148		
ANOVA						
Source of variation	SS	df	MS	F	P-value	F crit
Between groups	13066.011	8	1633.251	40.608	9.458E-16	2.2085
Within groups	1447.921	36	40.220			
Total	14513.932	44				

3.11. Compression test

The specimen's compressive strength as per ASTM D695 [41] was obtained using a Universal Testing Machine (Shimadzu AGS-50kNXD). Figure 31a,b illustrate the compressive strength values obtained by averaging the results of five specimens.

3.11.1. Compression test result for PLA-TPU with unmodified CNC

As shown in Figure 31a, PLA-TPU with unmodified CNC exhibits the highest compressive strength of all tested materials, measuring 13.2 MPa. Composites with unmodified CNC concentrations of 0.05% and 3% exhibit a slight decrease in compressive strength compared to PLA-TPU, due to weaknesses within the composite's infill structure that affect its mechanical performance. Furthermore, compared to PLA-TPU and PLA-TPU-CNC at 0.05% and 3%, this composite with a 1% CNC concentration exhibits a considerable improvement in strength, ranging from 120% to 153.8%. Composites with unmodified CNC at 3% were less valuable than composites with 1% CNC due to inconsistencies in the composite structure.

3.11.2. Compression test result for PLA-TPU with modified CNC

The concentration levels in the modified CNC group (0.05%, 1%, and 3%) had a significant influence compared to all concentrations in the unmodified CNC group. Moreover, the composite with modified CNC at a 0.05% concentration exhibits a 130%–296% increase in strength compared to pure PLA, PLA-TPU, and PLA-TPU with 3% CNC concentrations.

For the record, in Figure 31b, the modified CNC group showed that the PLA-TPU-CNC (1%) displayed the highest compressive strength among all the examined materials, achieving 18.1 MPa. This concentration increases compressive strength by 13.1% to 160% compared to the other levels at 0.05% and 3%, respectively. The composite with 3% CNC exhibits a 21.9% increase compared with the blended composite at 3% unmodified CNC, as well as a 16.2% increase in blended PLA-TPU.

By directly functionalizing the cellulose surface area through the interaction of hydroxyl groups, which comprise both negative and positive electrostatic charges, with HDTMA-Br as the surface-active agent material [15], the researchers acknowledge the outstanding mechanical performance of PLA-TPU with modified CNC [32,35]. Furthermore, it is indisputable that the modified CNC material achieves an outstanding dispersion with nonpolar, hydrophobic PLA and TPU due to its interfacial adhesion with the hydrophobic PLA-TPU characteristics [1–3,6,7,21].

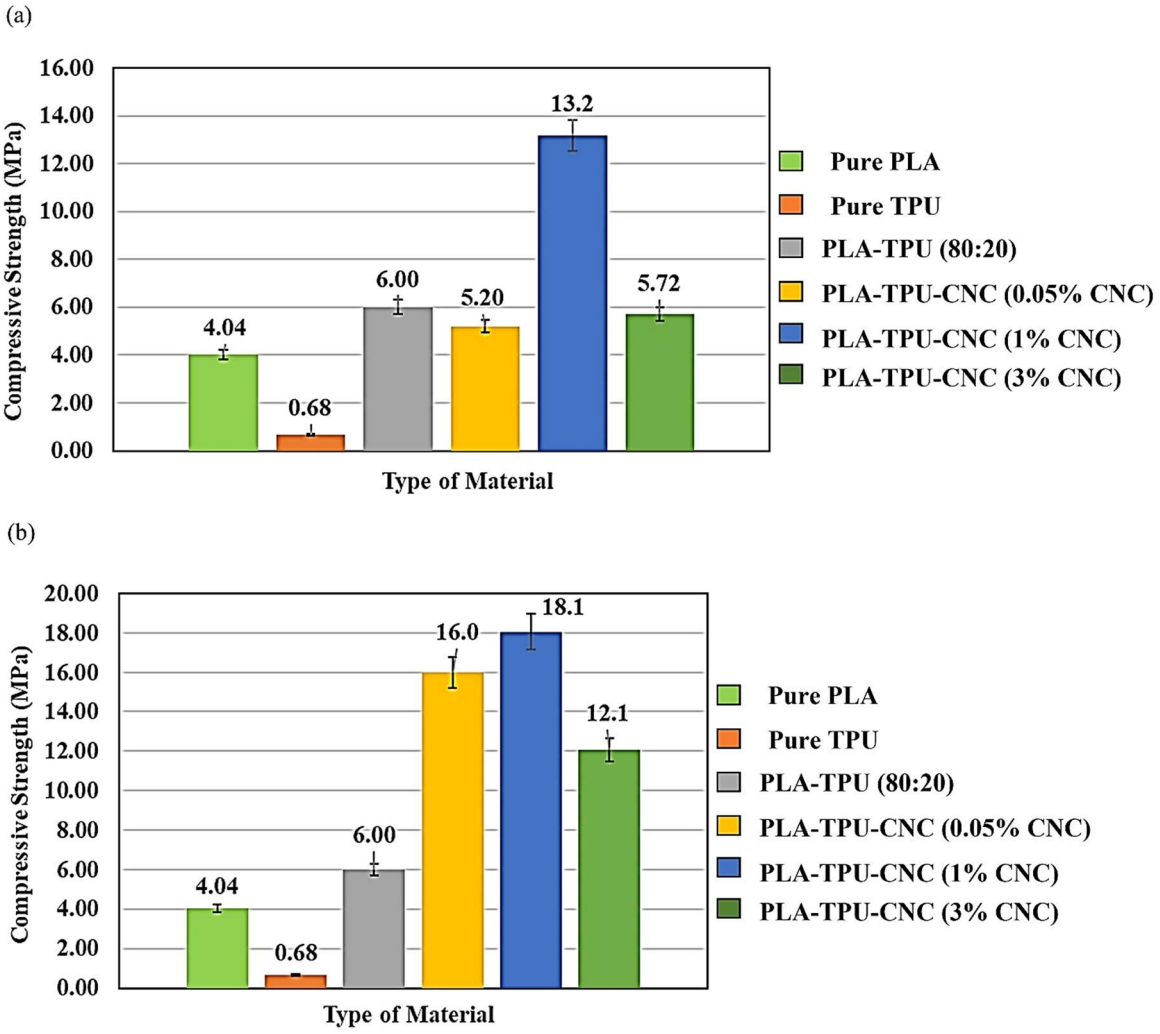

Figure 31. Compression test results for PLA-TPU with (a) unmodified CNC, and (b) modified CNC.

Figure 32a,b demonstrate that, of all the samples studied, pure PLA had the highest modulus of elasticity, measured at 644 MPa. This can be attributed to the material's underlying brittleness, which allowed it to achieve the lowest strain value.

On the other hand, thermoplastic polyurethane (TPU) has the lowest modulus of elasticity, with a value of 18.11 MPa. This can be attributed to the material's inherent flexibility, which resulted in the

highest strain value. Figure 32a,b show that the modulus of elasticity of both unmodified and modified composites decreases as CNC concentration increases. This is due to the cross-linking of TPU polymer chains employing both the unmodified and modified CNC [1–4,6,7].

Crosslinking creates covalent bonds between polymer chains, producing a more durable and long-lasting final product. Furthermore, when a strain is involved, the cross-linking activities of the TPU polymer chain remain more favorable with CNC than PLA, although PLA contributes 80% of the total PLA-TPU compound.

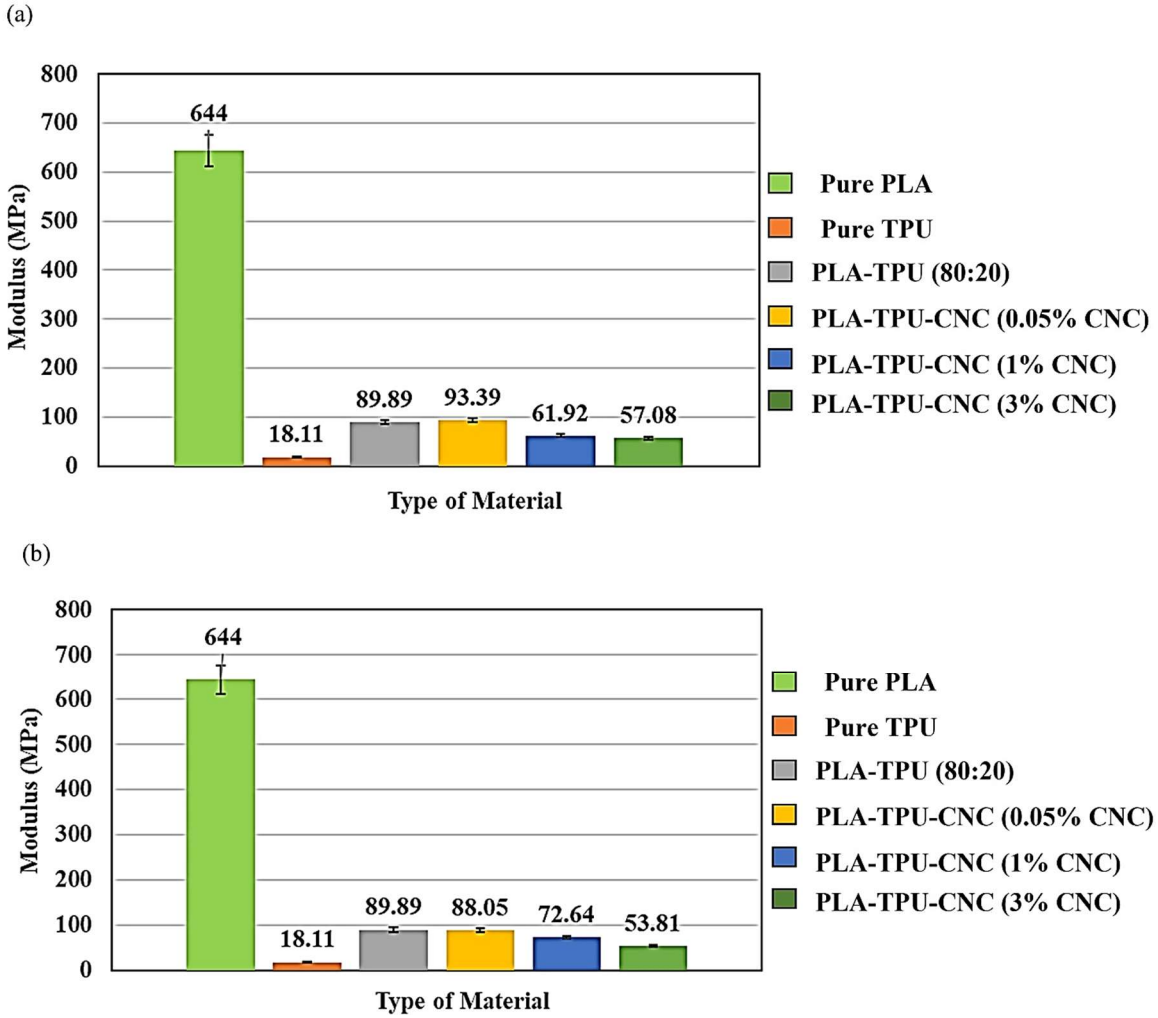

Figure 32. Modulus test results for PLA-TPU with (a) unmodified CNC, and (b) modified CNC.

Furthermore, PLA is a nonpolar and hydrophobic polymer, whereas TPU comprises chains with low-polarity segments [1–3,6,21,32].

The composite group of samples with modified CNC had a lower compressive modulus than the unmodified CNC group. This demonstrated that the cross-linking of polymer chains between the thermoplastic urethane and modified CNC is more favorable than that in the unmodified CNC group, opening the possibility of making the hydrophilic CNC more compatible with thermoplastic urethane [2,21].

Table 5. One-way ANOVA: compression test (MPa).

Summary						
Groups	Count	Sum	Average	Variance		
Pure PLA	5	20.1820	4.0364	1.06114		
Pure TPU	5	3.40600	0.6812	0.00188		
PLA-TPU	5	29.9768	5.9954	0.53476		
Unmodified CNC 0.05%	5	26.0031	5.2006	0.84456		
Unmodified CNC 1%	5	65.8637	13.173	10.9221		
Unmodified CNC 3%	5	28.6405	5.7281	6.29478		
Modified CNC 0.05%	5	80.0113	16.0023	6.69792		
Modified CNC 1%	5	90.4020	18.0804	3.16264		
Modified CNC 3%	5	34.8310	6.9662	14.6653		
ANOVA						
Source of variation	SS	df	MS	F	P-value	F crit
Between groups	1390.5500	8	173.8187	35.4049	8.243E-15	2.2085
Within groups	176.7405	36	4.9095			
Total	1567.2905	44				

The F-statistics for all levels of concentration in Table 5 exhibited a significant ratio of 35.40, surpassing the F-critical value of 2.21. Once again, the p-value obtained is ≤0.05, indicating that the design criteria between each group or level of concentration are statistically significant.

3.12. Heat deflection test

The deflection temperature was obtained according to ASTM D648 [42] to determine the flexural load of plastics. Figure 33a,b illustrate the heat deflection values obtained by averaging the results of two specimens. As shown in the figure, pure PLA exhibits the highest heat deflection of any of the materials tested, deflecting at 55.95 °C, in contrast to pure TPU, which deflected at only 37.6 °C due to its natural rubber-like flexibility.

3.12.1. Heat deflection test result for PLA-TPU with unmodified CNC

Furthermore, the heat deflection of PLA-TPU (80:20) and other composites with unmodified and modified CNC at concentrations of 0.05%, 1%, and 3% is quite similar to that of pure PLA. PLA-TPU-CNC, unmodified at 0.05% and 1%, exhibited a slight increase in heat deflection of 0.94% and 2.33%, respectively, compared to plain PLA-TPU (80:20). Similarly, at 1% CNC concentration, there was a slight increase in heat deflection, from 1.38% to 3.26%, when compared individually with unmodified CNC at 0.05% and 3% concentrations.

3.12.2. Heat deflection test result for PLA-TPU with modified CNC

The heat deflection temperature of PLA-TPU-CNC modified at 0.05% increased by 1.12% to 55.04 °C compared to plain PLA-TPU only. Moreover, the composite with modified CNC at 0.05% exhibits a slight increase, from 0.42% to 2.71%, when compared individually to modified CNC at 1% and 3% concentrations.

The reinforcing effect of CNC on PLA-TPU slightly improves the heat deflection of the entire composite structure. The formation of links between polymer chains within the structural composition of PLA-TPU-CNC, whether in modified or unmodified form, significantly enhances the material's thermal stability, making it more resistant to temperature fluctuations [43].

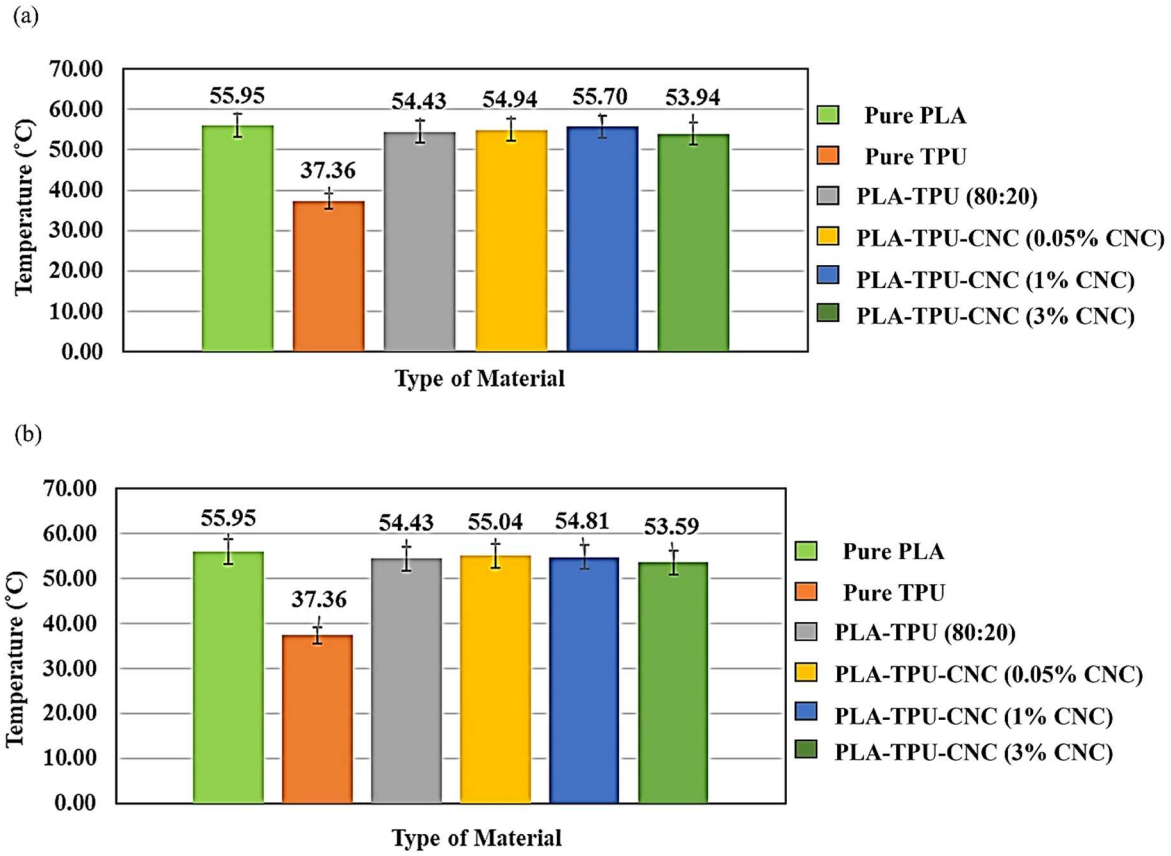

Figure 33. Heat deflection test results for PLA-TPU with (a) unmodified CNC and (b) modified CNC.

The F-statistics for all concentration levels in Table 6 yielded a significant ratio of 1253.1, significantly surpassing the F-critical value of 3.23. Once again, the p-value obtained is ≤5%, indicating that the design criteria between each group or level of concentration are statistically significant.

Table 6. One-way ANOVA: heat deflection test (°C).

Summary						
Groups	Count	Sum	Average	Variance		
Pure PLA	2	111.9	55.95	0.0008		
Pure TPU	2	74.72	37.36	0.0032		
PLA-TPU	2	108.86	54.43	0.0018		
Unmodified CNC 0.05%	2	109.87	54.94	0.2112		
Unmodified CNC 1%	2	111.41	55.71	0.0005		
Unmodified CNC 3%	2	107.89	53.95	0.0180		
Modified CNC 0.05%	2	110.09	55.05	0.0313		
Modified CNC 1%	2	109.61	54.81	0.0220		
Modified CNC 3%	2	107.18	53.59	0.2048		
ANOVA						
Source of variation	SS	df	MS	F	P-value	F crit
Between groups	549.860	8	68.732	1253.099	8.644E-13	3.2296
Within groups	0.494	9	0.055			
Total	550.354	17				

3.13. Hardness test

The indentation hardness of the materials was determined according to ISO 868 and ASTM D2240 [44,45]. The durometer hardness values shown in Figure 34a,b are averages of five specimens. As demonstrated in the figure, pure PLA exhibits the highest hardness of all the tested materials, with a Shore D hardness of 63.4.

3.13.1. Hardness test result for PLA-TPU with unmodified CNC

Additionally, compared to pure PLA, the reinforcing effect of unmodified CNC on the overall hardness structure of PLA-TPU is significantly smaller. From plain PLA-TPU to the other unmodified CNC concentration levels (0.05% and 1%), the hardness value climbs dramatically with increasing concentration. However, when compared with pure PLA, all modified CNC concentrations show exceptional hardness. With a 3% concentration of PLA-TPU-unmodified CNC, the hardness achieved was only 57.4 durometer, or approximately 8.95% less than pure PLA.

3.13.2. Hardness test result for PLA-TPU with modified CNC

The PLA-TPU with modified CNC at 0.05% achieves a hardness of 65.56 Shore D, with a 64.15% increase over PLA-TPU. PLA-TPU with modified CNC at 1% achieves a hardness of 68.22 Shore D, representing an 8.22% increase over pure PLA, which achieves a hardness of 63.04 Shore D. The modified CNC's reinforcing effect on PLA-TPU significantly improves the composite's hardness compared to pure PLA, as evidenced by its higher crystallinity index than the sample group with unmodified CNC. Although the blended composite at 3% modified CNC exhibited a slight difference

of 0.38 Shore D hardness compared to the composite at 1% modified CNC, it showed a remarkable hardness ranging from 3.36% to 41.13% when compared with pure PLA, PLA-TPU, and the composite with 0.05% modified CNC. The modified CNC at a 3% concentration contributes additional hardness to the PLA-TPU blend due to its interfacial cohesive adhesion with the matrix.

Furthermore, the modified CNC at 1% achieved the highest hardness attribute in his group and among the other unmodified CNC concentrations, TPU, and blended PLA-TPU. Similarly, PLA-TPU with 1% modified CNC yielded a 29.6% increase over the blended composite at 1% unmodified concentration.

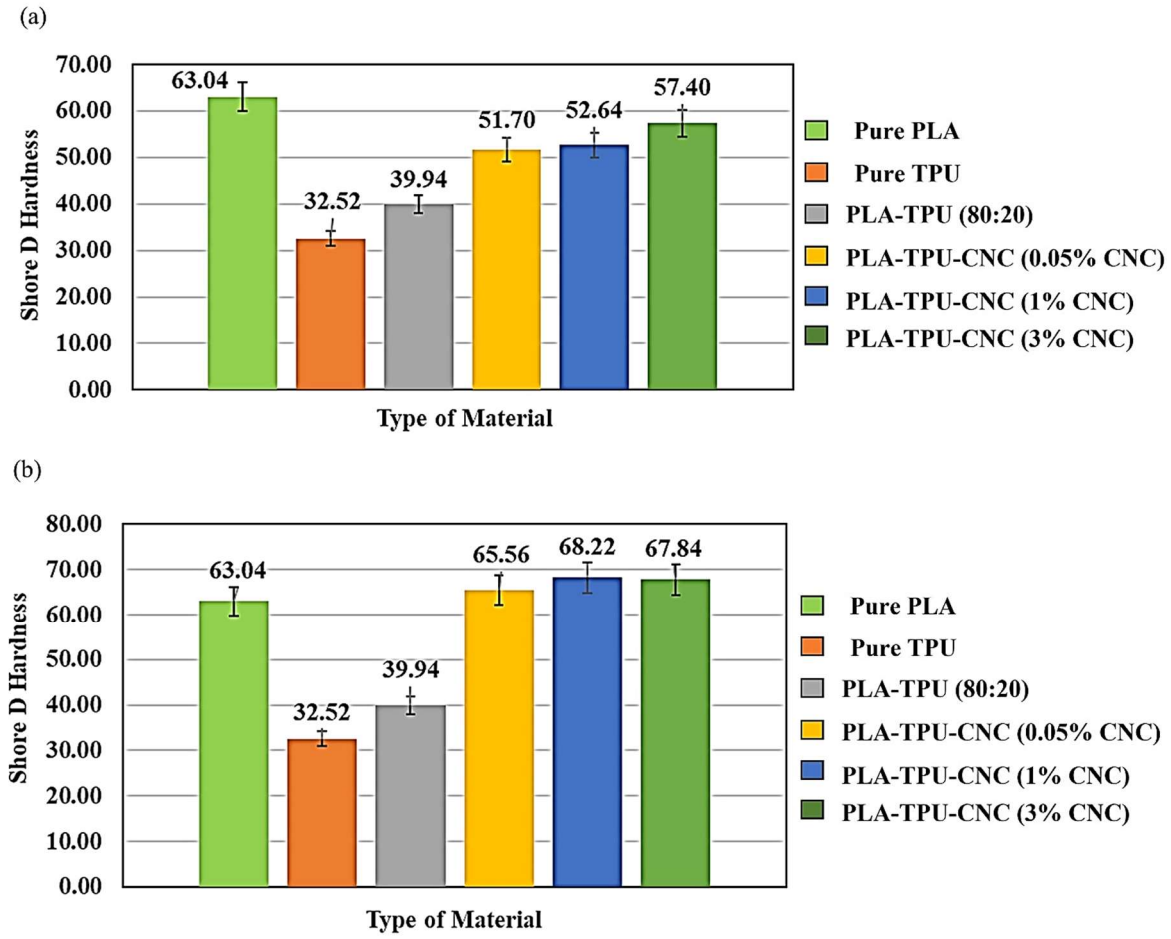

Figure 34. Hardness test results for PLA-TPU with (a) unmodified CNC and (b) modified CNC.

The F-statistics for all concentration levels in Table 7 yielded a significant ratio of 45.14, significantly surpassing the F-critical value of 2.21. Moreover, the p-value obtained was ≤5%, indicating that the design criteria between each group or level of concentration are statistically significant.

Table 7. One-way ANOVA: hardness test (Shore D hardness).

Summary						
Groups	Count	Sum	Average	Variance		
Pure PLA	5	315.2	63.04	0.1480		
Pure TPU	5	162.6	32.52	24.812		
PLA-TPU	5	199.7	39.94	36.498		
Unmodified CNC 0.05%	5	258.5	51.70	8.9850		
Unmodified CNC 1%	5	263.2	52.64	36.143		
Unmodified CNC 3%	5	287.0	57.40	22.105		
Modified CNC 0.05%	5	327.8	65.56	10.813		
Modified CNC 1%	5	341.1	68.22	10.067		
Modified CNC 3%	5	339.2	67.84	8.5180		
ANOVA						
Source of variation	SS	df	MS	F	P-value	F crit
Between groups	6342.536	8	792.817	45.135	1.740E-16	2.2085
Within groups	632.356	36	17.565			
Total	6974.892	44				

3.14. Influence of 3D printing parameters on the composite's structures and properties

Figure 35 demonstrates a 3D printing process using a fused deposition modeling printer to visualize the impact of each printing parameter as specified in Table 8.

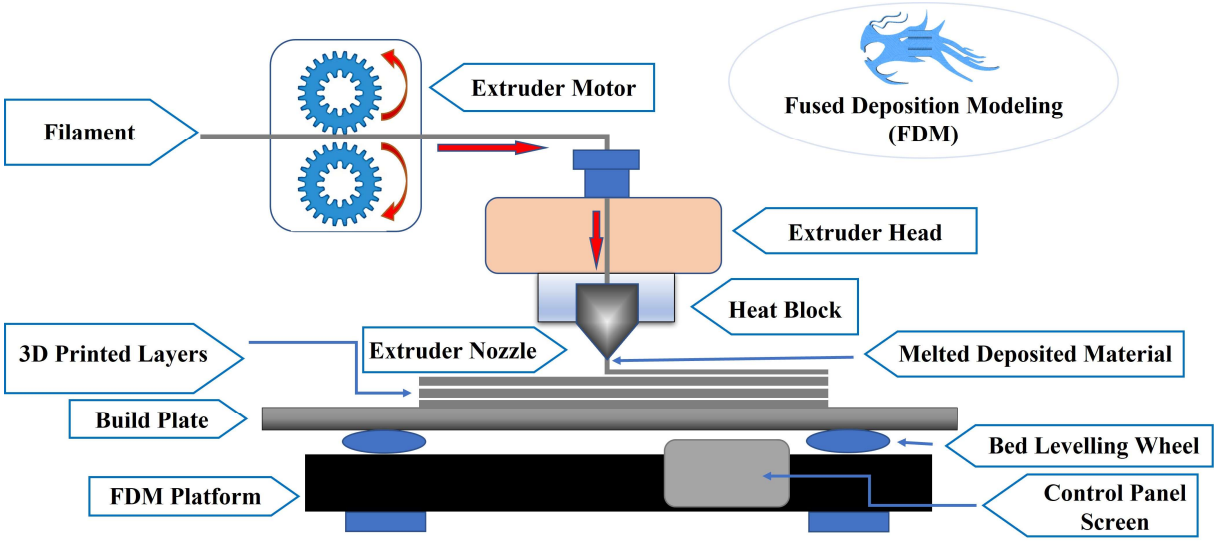

Figure 35. 3D printing process using a fused deposition modeling printer machine.

The smoothness of the 3D printing process determines the rigidity of a composite construction. A high porosity ratio, resulting in a large volume of voids, shows insufficient filling of extruded filament material from the nozzle. This is due to flow constraints inside the heat block. One probable

explanation for the unsmooth and uneven flow of extruded material is that the filament diameter is either inadequate or excessively large.

Furthermore, insufficient infill extrudate material impacts the quality and mechanical properties of 3D-printed composite materials. Table 8 provides a logical framework for examining the effect of printing parameters on the composite's structure and properties.

Table 8. Logical framework analysis on the effect of 3D-printing parameters on the composite's structure.

3D printing parameters	Description	Influence of 3D-printing parameters on composite structure	Preventive actions to improve the structure of 3D-printed specimens
Nozzle diameter	Exit orifice of the molten material	Possible obstruction of molten material from the orifice due to sticky residue in the nozzle and filament material in the heat block. Insufficient infill structure impacts both the mechanical and thermal performance of composites [30].	Consider regularly cleaning and replacing the nozzle after printing a sample with 3D printing. Consistently verify that the filament size is within the specified standard diameter range [30,31].
Raster angle	Angle between the deposited material and the x-axis	The raster angle has no adverse effect on the quality of the 3D-printed layer as long as the build plate levelling is consistently calibrated/levelled [30].	Consistently check and verify the build plate level before initiating 3D printing.
Perimeter's Overlapped.	There is an overlap between each layer.	The overlap in the study is 55%, ensuring no gaps are seen during the 3D printing of each layer. This parameter has no adverse effect on the quality of the 3D-printed layer [30].	Consider checking the appearance of each printed layer during the 3D printing process.
Raster width	Extruded material width	The smooth flow of the molten material also affects the geometrical size and shape of the raster width. Insufficient extruded material significantly impacts the composite's mechanical and thermal properties [30].	Check the feeding operations of the filament gears to ensure that the filament is continually pushed down to the nozzle. Additionally, verify the filament diameter [30,31].
Layer height/thickness	Extruded material thickness	The smooth flow of the molten material influences the geometric size and shape of the layer, including its height and thickness. The insufficient layer height or thickness significantly impacts the composite's mechanical and thermal characteristics [30].	Check the feeding operations of the filament gears to ensure that the filament is continually pushed down to the nozzle. Additionally, verify the filament diameter [30,31].

Continued on next page

3D printing parameters	Description	Influence of 3D-printing parameters on composite structure	Preventive actions to improve the structure of 3D-printed specimens
Printing speed	Material extrusion speed	According to Rahmatabadi et al., the study's extrusion rate affects the geometric shape and size of the printed layer. The study's extrusion speed ranges from 50 to 60 mm/s (the standard extrusion speed for PLA). However, because TPU requires a lower extrusion speed, it is possible that insufficient melting of the composite filament may affect the infill structure for each printed layer at speeds of 50 to 60 mm/s. Insufficient infill structure has a tangible impact on the composite's mechanical and thermal properties. The embedded CNC material, however, has a low concentration value and does not directly affect the printed shape and size of each layer.	The researchers can investigate using a slower extrusion speed to accomplish the specimen's optimum and desired infill structure. Future research can explore different extrusion speeds, particularly for this PLA-TPU composite, to enhance the smoothness and quality of 3D printing [30].
Nozzle temperature	Molten material temperature	The study's 230 °C nozzle extrusion temperature significantly improves the smoothness of the extruded composite material's flow. However, certain voids are visible inside the composite's infill structure in some cases, as seen in Figures 19 and 20 (SEM-EDX Image). The high porosity ratio has a significant impact on the composite's mechanical properties. Similarly, the DSC results showed that the degree of interfacial adhesion bonding between the modified CNC and the matrix contributed considerably to the composite's temperature transition and stability [30,31,37].	Future research investigations can account for differences in nozzle temperatures to assess the effect of porosity on the structure. Furthermore, Chen et al. reported 210 °C for PLA TPU mixes with fillers, while Rahmatabadi et al. reported 220 °C [30,37]
Build plate/platform temperature	Bedplate/workspace temperature	The study's 60 °C build plate temperature enables substantially more permanent surface bonding between the extruded layer of the composite material and the bedplate. However, certain voids are visible within the composite's infill structure for PLA-TPU with unmodified CNC in some cases, as seen in Figures 19 and 20 (SEM-EDX image). Similarly, the high porosity ratio significantly affects the composite's mechanical and thermal properties [30,37].	Future research studies can accommodate other variations for the build plate temperatures to determine the effect of porosity within the structure. Moreover, some studies for PLA-TPU blends with fillers used 60 °C, as mentioned by Chen et al. [2,30,37]

Continued on next page

3D printing parameters	Description	Influence of 3D-printing parameters on composite structure	Preventive actions to improve the structure of 3D-printed specimens
Infill density	Amount of melted material	The specimen's 20% infill structure, as shown in Figure 27b, was not completely achieved due to some common printing issues: Filament size variation, which sometimes resulted in clogging inside the heat block and nozzle, inefficient leveling of the build plate, and filament stuck inside the Bowden tube due to oversized or buckling of the filament. Insufficient infill structure has a significant impact on the composite's mechanical performance. In this situation, the tensile strength value obtained for PLA-TPU-CNC (unmodified) at 1% and 3% concentrations is lower than that of PLA-TPU alone [30,31].	The prepared filament is strongly recommended to meet standard size and dimension specifications similar to those of commercial filament. A water bath should also be explored to control the diameter of the filament. Check the build plate's condition regularly and adjust the leveling as needed. Always examine the filament's physical condition inside the Bowden tube and the feeding functionality of the filament gears [30,31].
Infill pattern	Infill material internal shape	Similar to the raster angle and perimeter overlap, the infill pattern is determined by the condition and behavior of the filament material, as well as the final configuration of all other parameters. Similarly, it has no adverse impact on the quality of the 3D-printed layer as long as the build plate levelling remains consistent. Nonetheless, the incomplete pattern can affect the target infill density, directly impacting the composite's mechanical and thermal properties [30].	Before 3D printing, consistently check and verify the filament condition and build plate level [30,37].

4. Conclusions

The coated structure of the HDTMA-Br surfactant adsorbed on CNC considerably reduced thermal energy compared to unmodified CNC. Thus, modified CNCs produce less exothermic energy than unmodified CNCs. The improved CNC and matrix improve the composite's thermal transition and stability, while a modest increase in T_g increases its structural stiffness. HDTMA-Br modification of CNC cellulose resulted in an enhanced crystalline structure with higher peak intensity, indicating increased atom contribution in the CNC crystal area and highly ordered crystals in cellulose. The cationic components of HDTMA-Br enhanced the modified CNC surface, leading to a more ordered crystal arrangement and a needle-like morphology with improved particle dispersion.

We found that irregularities in 3D printing and variations in filament diameter resulted in cavities in the 3D-printed part of a specimen. HDTMA-Br can alter the surface properties of CNC nanoparticles from hydrophilic to hydrophobic, thereby influencing their dispersion in the PLA-TPU matrix. Combining HDTMA-Br with cellulose nanocrystals enhanced the carbon content of CNCs while decreasing their oxygen concentration. Due to its compatibility with the surface of the structure, the modified CNC in PLA-TPU composite exhibits somewhat lower surface roughness than the unmodified CNC. Among all materials evaluated, PLA-TPU exhibited the maximum tensile strength at a 0.05% modified CNC content. The composite with modified CNC exhibits a significantly higher tensile strength (19.12 MPa) than the unmodified CNC. A cationic surfactant considerably improves the interaction between CNC and PLA-TPU. PLA-TPU with 3% modified CNC had the highest flexural strength at 52.36 MPa, representing a 58.3% improvement over unmodified CNC.

Using cationic surfactants such as HDTMA-Br improves CNC interfacial adhesion, necessitating careful control of CNC hydrophobicity. The modified CNC group substantially impacts the mechanical performance of PLA-TPU-CNC, exhibiting better interfacial adhesion and hydrophobic characteristics than the unmodified CNC groups at concentrations of 0.05%, 1%, and 3%. We found that PLA-TPU-CNC (1%) exhibited the highest compressive strength among the materials tested, with a value of 18.1 MPa. This was owing to the interaction of hydroxyl groups with HDTMA-Br, which improved the mechanical properties of PLA-TPU with modified CNC. The modified CNC material also dispersed well with non-polar hydrophobic PLA and TPU, indicating a positive cross-linking between thermoplastic urethane and modified CNC. Cellulose nanocrystal reinforcement in PLA-TPU enhances heat deflection and thermal stability, whereas modified or unmodified polymer chains increase resistance to temperature fluctuations.

We considered only the TG-DTA characterization test for unmodified and modified CNC. However, the effect on the composite's thermal properties was reported under the heat deflection temperature test. The maximum heat deflection range reached by the 3D-printed composite with unmodified and modified CNC will only fall from 53 to 56 °C. The deflection temperature of the composite specimen shall be measured upon reaching the 0.25 mm deflection at 0.455 MPa applied load as per ASTM D648. By more than 56 °C, the deflection of the composite is expected to reach more than 0.25 mm.

We discovered that unmodified CNC considerably decreases the hardness structure of PLA-TPU compared to pure PLA. With a 3% concentration, the hardness is 57.4 durometer, 8.95% lower than pure PLA. However, all modified CNC concentrations exhibit excellent hardness, with 1% modified CNC obtaining 68.22 durometer hardness, representing an 8.22% increase over pure PLA. This produces a 29.6% gain over the blended composite. Deviations in the diameter of the filament that affect the quality of 3D printing are slightly addressed in this research study to obtain the standard size requirement of 1.75 mm, consistent with a tolerance of 1.65 to 1.85 mm. However, an in-depth research method for a more precise and consistent composite filament preparation is recommended to achieve the desired standard size requirements nearly the same as the commercial filament. We also integrate a logical framework to assess the contribution of printing parameters and improve the mechanical and thermal properties of 3D printed composite material.

Reinforcing PLA-TPU with unmodified and modified CNC significantly improved the composite's mechanical and thermal properties. Moreover, optimizing various CNC concentrations revealed that adding 1% modified CNC significantly enhanced the mechanical properties and structural integrity of the PLA-TPU composite. The study's F-statistics consistently exceed the F-critical value,

indicating data points are close to each other. Furthermore, the p-value consistently falls below 0.05, indicating statistical significance in the design criteria used between each group or concentration level.

One possible application of this composite material is in medical and biosafety services, particularly in prosthetics, such as the transtibial prosthetic socket for amputees, where missing body parts are replaced with artificial ones. Suggestions for the composite material's long-term performance stability are also substantial in determining its long-term effect on the mechanical and thermal properties, specifically in the surrounding environment. Although this was not included in the current scope, it will be considered in future studies.

Use of AI tools declaration

The authors declare they have not used artificial intelligence (AI) tools in the creation of this article.

Author contributions

Paul Eric C. Maglalang: conceptualization, methodology, software, resources, data analysis and investigation, data collection, writing—original draft, writing—review and editing, and visualization. Blessie A. Basilia: conceptualization, methodology, research work assessment, review & editing, supervision, and overall administration.

Acknowledgments

The authors extend their appreciation to the Department of Science and Technology (DOST), Science Education Institute (SEI), and Mapua University for funding this research venture. We would also like to express our heartfelt gratitude to all of the staff and laboratories at the Industrial Technology Development Institute (ITDI—Department of Science and Technology) for their contributions to the success of this research study and its alignment with the Harmonized National Research and Development Agenda (HNRDA) "AmBisyon Natin 2040".

Conflict of interest

The authors declare that they have no conflict of interest.

References

1. Ambone T, Torris A, Shanmuganathan K (2020) Enhancing the mechanical properties of 3D-printed polylactic acid using nanocellulose. *Polym Eng Sci* 60: 1842–1855. https://doi.org/10.1002/pen.25421
2. Chen Q, Mangadlao JD, Wallat J, et al. (2017) 3D printing biocompatible polyurethane/poly(lacticacid)/graphene oxide nanocomposites: Anisotropic properties. *ACS Appl Mater Interfaces* 9: 4015–4023. https://doi.org/10.1021/acsami.6b11793
3. Rahmatabadi D, Ghasemi I, Baniassadi M, et al. (2022) 3D printing of PLA-TPU with different component ratios: Facture toughness, mechanical properties, and morphology. *J Mater Res Technol* 21: 3970–3981. https://doi.org/10.1016/j.jmrt.2022.11.024

4. Sharifah ISS, Adnan MDA, Nor Khairusshima MK, et al. (2018) Effect of thermoplastic polyurethane (TPU) on the thermal and mechanical properties of polylactic acid (PLA)/curcumin blends. *IOP Conf Ser Mater Sci Eng* 290: 012081. https://dx.doi.org/10.1088/1757-899X/290/1/012081
5. Marinopoulos T, Li S, Silberschmidt V (2021) Structural integrity of 3D-Printed prosthetic sockets: An experimental study for paediatric above-knee applications. *Procedia Struct Integr* 37: 139–144. https://doi.org/10.1016/j.prostr.2022.01.069
6. Hong H, Wei J, Yuan Y, et al. (2011) A novel composite combines the hardness of polylactic acid with the flexibility of thermoplastic polyurethane. *J Appl Polym Sci* 121: 855–861. https://doi.org/10.1002/app.33675
7. Tran VH, Kim JD, Kim JH, et al. (2020) Influence of cellulose nanocrystal on the cryogenic mechanical behavior and thermal conductivity of polyurethane composite. *J Environ Polym Degrad* 28: 1169–1179. https://doi.org/10.1007/s10924-020-01673-3
8. Seppala JE, Hoon Han S, Hillgartner KE, et al. (2017) Weld formation during material extrusion additive manufacturing. *Soft Matter* 13: 6761–6769. https://doi.org/10.1039/C7SM00950J
9. Gurrala PK, Regalla SP (2014) Part strength evolution with bonding between filaments in fused deposition modelling. *Virtual Phys Prototyp* 9: 141–149. https://doi.org/10.1080/17452759.2014.913400
10. Bhalodi D, Zalavadiya K, Gurrala PK (2019) Influence of temperature on polymer parts manufactured by fused deposition modeling process. *J Brazilian Soc Mech Sci Eng* 41: 1–11. https://doi.org/10.1007/S40430-019-1616-Z
11. Cao Q, Cai Y, Jing B, et al. (2006) Structure and mechanical properties of thermoplastic polyurethane based on hyperbranched polyesters. *J Appl Polym Sci* 102: 5266–5273. https://doi.org/10.1002/APP.24779
12. Jing X, Mi HY, Peng XF, et al. (2015) The morphology, properties, and shape memory behavior of polylactic acid/thermoplastic polyurethane blends. *Polym Eng Sci* 55: 70–80. https://doi.org/10.1002/pen.23873
13. Tao Y, Kong F, Li Z, et al. (2021) A review on voids in 3D-printed parts by fused filament fabrication. *J Mater Res Technol* 15: 4860–4879. https://doi.org/10.1016/J.JMRT.2021.10.108
14. Ghorbani J, Koirala P, Shen YL, et al. (2022). Eliminating voids and reducing mechanical anisotropy in fused filament fabrication parts by adjusting the filament extrusion rate. *J Manuf Process* 80: 651–658. https://doi.org/10.1016/J.JMAPRO.2022.06.026.14
15. Kaboorani A, Riedl B (2015) Surface modification of cellulose nanocrystals (CNCs) with a cationic surfactant. *Ind Crop Prod* 65: 45–55. https://doi.org/10.1016/j.indcrop.2014.11.027
16. Mazzanti V (2019) FDM 3D printing of polymers containing natural fillers: A review of their mechanical properties. *Polymers* 11: 1–22. https://doi.org/10.3390/polym11071094
17. Dizon JRC, Espera AH, Chen Q, et al. (2018) Mechanical characterization of 3D-printed polymers. *Addit Manuf* 20: 44–67. https://doi.org/10.1016/j.addma.2017.12.002
18. Bhagia S, Bornani K, Agarwal R, et al. (2021) Critical review of FDM 3D printing of PLA biocomposites filled with biomass resources, characterization, biodegradability, upcycling, and opportunities for biorefineries. *Appl Mater Today* 24: 101078. https://doi.org/10.1016/j.apmt.2021.101078

19. Karimah A, Ridho MR, Munawar SS, et al. (2021) A review on natural fibers for development of eco-friendly bio-composite: Characteristics, and utilizations. *J Mater Res Technol* 13: 2442–2458. https://doi.org/10.1016/j.jmrt.2021.06.014
20. Kim S, Yalla S, Shetty S, et al. (2022) 3D printed transtibial prosthetic sockets: A systematic review. *PLoS One* 17: e0275161. https://doi.org/10.1371/journal.pone.0275161
21. Mondal S (2020) Cellulose nanocrystals as a prospective reinforcement for polymer matrix nanocomposites, In: Hashmi S, Choudhury IA, *Encyclopedia of Renewable and Sustainable Materials*, Oxford: Elsevier, 42–53. https://doi.org/10.1016/b978-0-12-803581-8.11292-5
22. Santos RM, Flausino Neto WP, Silvério HA, et al. (2013) Cellulose nanocrystals from pineapple leaf, a new approach for the reuse of this agro-waste. *Ind Crop Prod* 50: 707–714. https://doi.org/10.1016/j.indcrop.2013.08.049
23. Theivasanthi T, Christma FA, Toyin AJ, et al. (2018) Synthesis and characterization of cotton fiber-based nanocellulose. *Int J Biol Macromol* 109: 832–836. https://doi.org/10.1016/j.ijbiomac.2017.11.054
24. Kian LK, Jawaid M, Ariffin H, et al. (2018) Isolation and characterization of nanocrystalline cellulose from roselle-derived microcrystalline cellulose. *Int J Biol Macromol* 114: 54–63. https://doi.org/10.1016/j.ijbiomac.2018.03.065
25. Karimah A, Ridho MR, Munawar SS, et al. (2021) A review on natural fibers for development of eco-friendly bio-composite: characteristics, and utilizations. *J Mater Res Technol* 13: 2442–2458. https://doi.org/10.1016/j.jmrt.2021.06.014
26. Girijappa YG, Rangappa SM, Parameswaranpillai V, et al. (2019) Natural fibers as a sustainable and renewable resource for the development of eco-friendly composites: A comprehensive review. *Front Mater* 6: 1–14. https://doi.org/10.3389/fmats.2019.00226
27. Joshi SV, Drzal LT, Mohanty AK, et al. (2004) Are natural fiber composites environmentally superior to glass fiber reinforced composites? *Compos Part A Appl Sci Manuf* 35: 371–376. https://doi.org/10.1016/j.compositesa.2003.09.016
28. Moon RJ, Martini A, Nairn J, et al. (2011) Cellulose nanomaterials review: Structure, properties and nanocomposites. *Chem Soc Rev* 40: 3941–3994. https://doi.org/10.1039/C0CS00108B
29. Phanthong P, Reubroycharoen P, Hao X, et al. (2018) Nanocellulose: Extraction and application. *Carbon Resour Convers* 1: 32–43. https://doi.org/10.1016/j.crcon.2018.05.004
30. Thirugnanasambandam A, Dutta H, Gnanasagaran CL, et al. (2025) Development of 3D printed novel multi-polymer component based on blended filaments of polylactic acid and polyethylene terephthalate glycol. *Prog Addit Manuf* 10: 1147–1160. https://doi.org/10.1007/s40964-024-00695-w
31. Kechagias JD (2022) Materials for additive manufacturing. *AIMS Mater Sci* 9: 785–790. https://doi.org/10.3934/matersci.2022048
32. Ly M, Mekonnen T (2019) Cationic surfactant modified cellulose nanocrystals for corrosion protective nanocomposite surface coatings. *J Ind Eng Chem* 83: 409–420. https://doi.org/10.1016/j.jiec.2019.12.014
33. Xie J, Liu S (2021) A review of hydrophobic nanocellulose and its applications. *Pap Biomater* 6: 35–42. https://doi.org/10.12103/j.issn.2096-2355.2021.02.004
34. Mattia I (2024) Thermal properties and decomposition products of modified cotton fibers, as determined by TGA, DSC, and Py–GC/MS. *Polym Degrad Stab* 228: 2–12. https://doi.org/10.1016/j.polymdegradstab.2024.110937

35. Rasheed M, Jawaid M, Parveez B, et al. (2020) Morphological, chemical, and thermal analysis of cellulose nanocrystals extracted from bamboo fiber. *Int J Biol Macromol* 160: 183–191. https://doi.org/10.1016/j.ijbiomac.2020.05.170
36. Kaushik M, Fraschini C, Chauve G, et al. (2015) Transmission electron microscopy for the characterization of cellulose nanocrystals, In: Maaz K, *The Transmission Electron Microscope—Theory and Applications*, Rijeka: IntechOpen, 130–163. https://doi.org/10.5772/60985
37. Kechagias J, Zaoutsos S (2024) Effects of 3D printing processing parameters on FFF parts' porosity: Outlook and trends. *Mater Manuf Process* 39: 804–814. https://doi.org/10.1080/10426914.2024.2304843
38. ASTM International (2014) Standard test method for tensile properties of plastics. ASTM D638-14.
39. ASTM International (2015) Standard test methods for flexural properties of unreinforced and reinforced plastics and electrical insulating materials. ASTM D790-15e2.
40. ASTM International (2010) Standard test methods for determining the Izod pendulum impact resistance of plastics. ASTM D256-10e1.
41. ASTM International (2015) Standard test method for compressive properties of rigid plastics. ASTM D695-15.
42. ASTM International (2007) Standard test method for deflection temperature of plastics under flexural load in the edgewise position. ASTM D648-07.
43. Vigneshwaran S (2024) The thermal properties of FDM printed polymeric materials: A review. *Polym Degrad Stab* 228: 1–19. https://doi.org/10.1016/j.polymdegradstab.2024.110902
44. ISO Standard (2003) Plastics and ebonite—Determination of indentation hardness using a durometer—Shore hardness (ISO 868-03), Case postale 56 CH-1211 Geneva 20.
45. ASTM International (2015) Standard test method for rubber property—Durometer hardness. ASTM D2240-15.

AIMS Press